Accurate heat (Fourier) and mass (Fick and thermodiffusion) multicomponent transport at similar cost as mixture-averaged approximation

Bertrand Naud*[a], Oscar Córdoba[b], Manuel Arias-Zugasti[b]

[a]Modelling and Numerical Simulation Group, Energy Department, CIEMAT, Avda. Complutense 40, 28040 Madrid, Spain
[b]Departamento de Física Matemática y de Fluidos, Facultad de Ciencias Universidad Nacional de Educación a Distancia (UNED), Av. de Esparta s/n, Carretera de Las Rozas al Escorial km 5, Las Rozas, 28232 Madrid, Spain

Abstract

An "extended $1 + M$ model" for Fick diffusion and thermodiffusion is proposed as a combination of both the efficient $1 + M$ model for Fick diffusion by Naud and Arias-Zugasti (2020), and an extension of the recent efficient multicomponent thermodiffusion formulation of Córdoba and Arias-Zugasti (2022). This new accurate and efficient model is mainly based on two ideas: proper re-scaling, enabling accurate and efficient inversion formulae based on Neumann series, and problem size reduction based on local identification of "main species". Calculations of steady and unsteady 1D counterflow flames prove the excellent accuracy of the model. Considering the evaluation of Fick and thermal diffusion coefficients and thermal conductivity, together with the efficient approximation for molecular viscosity, the model appears to have a similar cost as the standard mixture-averaged approximation, being even cheaper for large numbers of species. Compared to the complete multicomponent formulation, the cost is reduced by an order of magnitude with a 58-species mechanism and by two orders of magnitude with 202-species and 300-species mechanisms.

Key words: Differential diffusion, multicomponent gases, Fick diffusion, thermodiffusion, thermal conductivity, Kinetic Theory of Gases, mixture-averaged

1. Introduction

Based on the work of Monchick and Mason who generalised the Kinetic Theory of Gases to polyatomic molecules [1, 2, 3], we refer to Dixon-Lewis [4, 5] in order to describe molecular transport in the context of reacting flows. In order to evaluate thermal diffusion coefficients and thermal conductivity, a system $\mathbb{L}.\mathbf{a} = \mathbf{X}$ needs to be solved where $\mathbb{L}$ is a $(3N - n^\star) \times (3N - n^\star)$ matrix and where $\mathbf{a}$ and $\mathbf{X}$ are vectors of dimension $(3N - n^\star)$. N is the number of species considered, and $n^\star$ is the number of monatomic species (molecules which are single atoms: H, O, C, and possibly Ar or He). At the same time, the evaluation of multicomponent Fick diffusion coefficients requires the inversion of a $N \times N$ matrix, which corresponds to the first block $\mathbb{L}^{00,00}$ of matrix $\mathbb{L}$.

Since the dimension of this system may be large when considering problems involving many species, different approaches have been proposed in order to obtain accurate approximations of the multicomponent Fick diffusion problem at a lower cost than directly inverting the $N \times N$ matrix $\mathbb{L}^{00,00}$, and accurate approximations of the multicomponent thermodiffusion problem at a lower cost than directly solving $\mathbb{L}.\mathbf{a} = \mathbf{X}$. In particular, the work of Giovangigli and coworkers focused on conjugate gradient methods [6, 7, 8]. A different approach for Fick multicomponent diffusion was proposed by Xin *et al*. [9] where they reduced the matrix to be inverted by considering only the important species regarding Fick diffusion and where they used the mixture-averaged approximation for the other species. Ambikasaran and Narayanaswamy [10] considered the reduction of the multicomponent diffusion problem from a different perspective by noting that the matrix of the reciprocal of the binary coefficients $(1/\mathcal{D}_{ij})$ is a low-rank matrix, allowing the use of a fast low-rank matrix factorisation at a computational complexity of $O(N)$. From another point of view, in the context of the mixture-averaged approximation, Sun and Ju [11] reduced the number of species in the problem by eliminating redundant transport property calculations based on correlated groups with similarities in phase space.

All these different approaches could be used for instance in Direct Numerical Simulations, and possibly combined with efficient implementations of multicomponent transport as in [12, 13]. We consider here the approach followed by Arias-Zugasti and coworkers. As a starting point, Arias-Zugasti *et al*. [14] reformulated the multicomponent Fick problem in order to avoid to invert the $N \times N$ matrix $\mathbb{L}^{00,00}$, using Neumann series approximations after proper rescaling. In particular, they proposed their so-called $1 + M$ model, combining low-order Neumann series approximations for the most diluted species and inversion of a small $M \times M$ matrix in order to obtain the Fick diffusion coefficients.

Naud and Arias-Zugasti [15] considered the lowest order $1 + M$ model (using the approximation at order 0 for the dilute species), and proposed an implementation where the $\mathcal{N}_M$ main species are evaluated locally ($\mathcal{N}_M = 1 + M$). This formulation is somehow similar to the reduced multicomponent diffusion model proposed by Xin *et al*. [9], with the advantage

*Corresponding author
Email address: bertrand.naud@ciemat.es (Bertrand Naud)

that the $\mathcal{N}_M$ main species are defined locally and that not all binary diffusion coefficients need to be evaluated, and where no correction velocity needs to be added in order to ensure the net species diffusion flux to be zero. Moreover, using the definition of the $\mathcal{N}_M$ main species, they also proposed an efficient evaluation of molecular viscosity leading to a formulation of multicomponent Fick diffusion at a similar cost as the standard mixture-averaged approximation.

Córdoba and Arias-Zugasti [16] recently proposed a new efficient resolution of $\mathbb{L}.\mathbf{a} = \mathbf{X}$. By writing the system in terms of block matrices (see C), they formulated the multicomponent thermodiffusion problem as the inversion of two $N\times N$ matrices, where the first matrix inverse $\boldsymbol{\mathcal{L}}^{-1}$ (inverse of matrix $\mathbb{L}^{00,00}$) is already available from the evaluation of multicomponent Fick diffusion coefficients. Moreover, with an appropriate rescaling of matrix $\mathbb{L}$, they avoid the inversion of the second matrix $\boldsymbol{\mathcal{L}}_T$ by using Neumann series approximations at a given order of truncation.

In this paper, we propose to further improve the efficiency of the evaluation of thermal diffusion coefficients and thermal conductivity proposed by Córdoba and Arias-Zugasti [16], by taking advantage of the efficient $1+M$ approximation. First, the inverse matrix $\boldsymbol{\mathcal{L}}^{-1}$ and the approximation for molecular viscosity are obtained as in [15]. Second, the size of the system $\mathbb{L}.\mathbf{a} = \mathbf{X}$ is reduced to $(3\mathcal{N}_M - n_M^\star - 1)\times(3\mathcal{N}_M - n_M^\star - 1)$ by considering the $\mathcal{N}_M = 1 + M$ main species defined locally. In the evaluation of $\boldsymbol{\mathcal{L}}^{-1}$ a $M \times M$ matrix needs to be directly inverted together with an additional number of multiplications of the order of $M^2(N - M - 1)$ from the Neumann approximation at order 0 for dilute species. An approximation with Neumann series at order 3 is used to approximate the second $\mathcal{N}_M \times \mathcal{N}_M$ inverse matrix.

In the following, we first recall the general multicomponent formulation for both Fick diffusion fluxes and thermodiffusion fluxes, and we detail the specific form of the proposed extended $1 + M$ model. The steady and unsteady 1D counterflow diffusion flame formulations used to evaluate the model are then described. Results are presented for different mixtures, using different chemical mechanisms, in order to assess the accuracy and efficiency of the extended $1 + M$ model compared to both standard full multicomponent formulation and mixture-averaged approximation. For completeness, different appendices give details on the evaluation of transport properties, on multicomponent matrices, on block matrix operations leading to the formulation by Córdoba and Arias-Zugasti [16], on the mixture-averaged approximation and on a methane oxidation skeletal mechanism used in the calculations.

2. Multicomponent transport

2.1. Diffusion coefficients and thermal conductivity

The diffusion flux for species i is considered here as the sum of the Fick diffusion flux and the thermodiffusion flux (also referred to as thermophoresis or Ludwig-Soret transport):

$$\rho\mathbf{V}_i Y_i = -\rho Y_i \sum_j D_{ij}\mathbf{d}_j - \rho Y_i D_{T,i}\nabla\ln T \tag{1}$$

where ρ is the density of the mixture, T is the temperature, $\mathbf{V}_i$ is the diffusion velocity of species i and Y_i is the mass fraction of species i. In this paper, we will consider the simplest form of the Fick diffusion driving force vector $\mathbf{d}_j = \nabla X_j$, expressed as the gradient of mole fraction X_j.

In order to obtain the diffusion fluxes, we need to evaluate the Fick diffusion coefficients D_{ij} and the thermal diffusion coefficients $D_{T,i}$. Moreover, in order to solve the energy equation or temperature equation, the thermal conductivity λ is required.

Since the sum of species fluxes must be zero, it is sufficient to consider the fluxes for $N - 1$ species. By treating separately a given species K, for $i \neq K$, Equation (1) can then be written as:

$$\rho\mathbf{V}_i Y_i = -\rho\frac{W_i}{\overline{W}}\sum_{j\neq K} D_{ij}^\star\mathbf{d}_j - \rho\frac{W_i}{\overline{W}}D_{T,i}^\star\nabla\ln T \tag{2}$$
$$\text{with } D_{ij}^\star = X_i\left(D_{ij} - D_{iK}\right) \text{ and } D_{T,i}^\star = X_i D_{T,i}$$

where we used the relation between mass fractions and mole fractions $W_i X_i = \overline{W} Y_i$, with W_i the molar weight of species i and $\overline{W}$ the molar weight of the mixture.

2.2. Standard Dixon-Lewis formulation

Based on the developments by Monchick and Mason generalising the Kinetic Theory of Gases to polyatomic molecules [1, 2, 3], we will refer to the formulation of Dixon-Lewis [4] in the context of reacting gases. The multicomponent thermodiffusion problem consists in resolving:

$$\mathcal{K}\begin{pmatrix}\mathbb{L}^{00,00} & \mathbb{L}^{00,10} & \mathbb{0}\\ \mathbb{L}^{10,00} & \mathbb{L}^{10,10} & \mathbb{L}^{10,01}\\ \mathbb{0} & \mathbb{L}^{01,10} & \mathbb{L}^{01,01}\end{pmatrix}\begin{pmatrix}\mathbf{a}_{00}\\ \mathbf{a}_{10}\\ \mathbf{a}_{01}\end{pmatrix} = \begin{pmatrix}\mathbf{0}\\ \mathbf{X}\\ \mathbf{X}\end{pmatrix} \tag{3}$$

where $\mathbf{X}$ is the vector of the N species mole fractions, and where the constant $\mathcal{K}$ and the sub-matrices $\mathbb{L}^{mn,pq}$ can be expressed following Dixon-Lewis [4], and are detailed in B.

The Fick multicomponent diffusion coefficients are obtained in terms of $\boldsymbol{\mathcal{L}}^{-1}$, the inverse of $\mathbb{L}^{00,00}$, as:

$$D_{ij} = \left((\mathcal{L}^{-1})_{ij} - (\mathcal{L}^{-1})_{ii}\right) \tag{4}$$

The thermal diffusion coefficients $D_{T,i}$ and the thermal conductivity λ are obtained in terms of the solution of the system of equations (3) as

$$D_{T,i} = 2.5\mathcal{K}a_{00,i} \tag{5}$$

$$\lambda = -4\sum_{i=1}^{N} X_i\left(a_{10,i} + a_{01,i}\right) \tag{6}$$

2.3. Approximations by Arias-Zugasti and coworkers

Following Arias-Zugasti *et al.* [14] and Córdoba and Arias-Zugasti [16], the species K with largest concentration is removed from the first block of matrix $\mathbb{L}$. The new system is written in terms of a matrix $\widehat{\mathbb{L}}$ such that $\widehat{\mathbb{L}^{00,00}}$ is reduced to a $(N - 1)\times(N - 1)$ matrix. The difference between $\widehat{\mathbb{L}}$ and $\mathbb{L}$ is

that line K is removed from the first block line, and that the first block column reads

$$\widehat{L}_{ij}^{00,00} = L_{ij}^{00,00} - \frac{X_j W_j}{X_k W_K} L_{iK}^{00,00} \tag{7}$$

$$\widehat{L}_{ij}^{10,00} = L_{ij}^{10,00} - \frac{X_j W_j}{X_k W_K} L_{iK}^{10,00} \tag{8}$$

The system is then rescaled as follows:

$$F_{ij}^{mn,pq} = \lambda_i^{(mn)} \mu_j^{(pq)} \widehat{L}_{ij}^{mn,pq} \tag{9}$$

$$\widetilde{a}_{pq,j} = \frac{\mathcal{K}}{\mu_j^{(pq)}} a_{pq,j} \tag{10}$$

$$\widetilde{X}_{mn,i} = \lambda_i^{(mn)} X_i \tag{11}$$

with

$$\lambda_i^{(00)} = 1 \qquad \lambda_i^{(10)} = \frac{1}{L_{ii}^{10,10}} \qquad \lambda_i^{(01)} = \frac{1}{L_{ii}^{01,01}} \tag{12}$$

$$\mu_j^{(00)} = \frac{\mathcal{D}_{jK}}{X_j} \qquad \mu_j^{(10)} = 1 \qquad \mu_j^{(01)} = 1 \tag{13}$$

with $\mathcal{D}_{ij}$ the binary diffusion coefficients, such that (3) takes the form:

$$\begin{pmatrix} \mathbb{1} + \mathbb{A} & \mathbb{F}^{00,10} & \mathbb{0} \\ \mathbb{F}^{10,00} & \mathbb{F}^{10,10} & \mathbb{F}^{10,01} \\ \mathbb{0} & \mathbb{F}^{01,10} & \mathbb{1} \end{pmatrix} \begin{pmatrix} \widetilde{\mathbf{a}}_{00} \\ \widetilde{\mathbf{a}}_{10} \\ \widetilde{\mathbf{a}}_{01} \end{pmatrix} = \begin{pmatrix} \mathbf{0} \\ \widetilde{\mathbf{X}}_{10} \\ \widetilde{\mathbf{X}}_{01} \end{pmatrix} \tag{14}$$

The Fick multicomponent diffusion coefficients can be obtained from the inverse of the $(N-1)\times(N-1)$ matrix $\mathbb{1} + \mathbb{A}$:

$$c_{ij} = (\mathbb{1} + \mathbb{A})_{ij}^{-1} \quad \text{such that} \quad D_{ij}^{\star} = \mathcal{D}_{iK} c_{ij} \tag{15}$$

with $D_{ij}^{\star}$ defined in (2). In the formulation of Arias-Zugasti *et al.* [14], M "main" species are defined in addition to species K. Rows and columns of matrix $\mathbb{A}$ are reordered such that different block matrices are defined, $\mathbb{A}_{11}$, $\mathbb{A}_{12}$ and $\mathbb{A}_{22}$:

$$A_{11,ij} = \sum_k X_k \left(\frac{\mathcal{D}_{iK}}{\mathcal{D}_{ik}} - 1 \right) \delta_{ij} + X_i \left(\frac{W_j}{W_K} - \frac{\mathcal{D}_{iK}}{\mathcal{D}_{ij}} \right) \frac{\mathcal{D}_{jK}}{\mathcal{D}_{iK}} \tag{16}$$

$$A_{12,ij} = X_i \left(\frac{W_j}{W_K} - \frac{\mathcal{D}_{iK}}{\mathcal{D}_{ij}} \right) \frac{\mathcal{D}_{jK}}{\mathcal{D}_{iK}} \tag{17}$$

$$A_{22,ij} = \sum_k X_k \left(\frac{\mathcal{D}_{iK}}{\mathcal{D}_{ik}} - 1 \right) \delta_{ij} \tag{18}$$

where the sums are over the main species, and where the $M \times M$ matrix $\mathbb{A}_{11}$ corresponds to main species, the $M \times (N-M-1)$ matrix $\mathbb{A}_{12}$ corresponds to main species i and dilute species j, and the $(N-M-1)\times(N-M-1)$ matrix $\mathbb{A}_{22}$ is diagonal and corresponds to dilute species.

The lowest order $1+M$ model can be used as in Naud and Arias-Zugasti [15] to obtain an approximation of c_{ij}, such that for main species i and j

$$c_{ij} = [\mathbb{1} + \mathbb{A}_{11}]_{ij}^{-1} \tag{19}$$

for main species i and dilute species j

$$c_{ij} = -\left[(\mathbb{1} + \mathbb{A}_{11})^{-1} . \mathbb{A}_{12} . (\mathbb{1} + \mathbb{A}_{22})^{-1} \right]_{ij} \tag{20}$$

and for dilute species i

$$c_{ii} = [\mathbb{1} + \mathbb{A}_{22}]_{ii}^{-1} = 1 \Big/ \sum_k X_k \left(\frac{\mathcal{D}_{iK}}{\mathcal{D}_{ik}} - 1 \right) \tag{21}$$

In this case, we only need to invert a $M \times M$ matrix in (19), where M is the number of "main" species verifying

$$X_i \geq \gamma X_K \tag{22}$$

with $\gamma = 10^{-5}$ [15]. Moreover, since $(\mathbb{1} + \mathbb{A}_{22})^{-1}$ is diagonal, only one block matrix multiplication needs to be performed in (20) (M multiplications for each $M(N-M-1)$ coefficients c_{ij}).

Note that in this approach the number of so-called "main" species $\mathcal{N}_M = 1 + M$ is not small in the flame zone with the value $\gamma = 10^{-5}$. For instance, in [15] the maximum value of $\mathcal{N}_M$ was 22 in a methane flame using a 57-species mechanism, and it was 63 in a *n*-dodecane flame using a 255-species mechanism. However, in practical combustion applications, the volume of the flame zone (where $\mathcal{N}_M$ may not be too small) is a reduced portion of the total volume of the problem (where $\mathcal{N}_M$ is mostly small). Still, in parallel computations based on domain decomposition, a strategy will need to be established in order to make sure that the flame zones are distributed over the different processors.

As detailed in C, following Córdoba and Arias-Zugasti [16], an approximation at order n of thermal diffusion coefficients and thermal conductivity can be obtained. This approximation can be written in terms of $\widehat{L}_{ij}^{10,00}$, $L_{ij}^{00,10}$, $L_{ij}^{10,10}$, $L_{ij}^{10,01}$ and $F_{ij}^{01,10} = L_{ij}^{01,10} / L_{ii}^{01,01}$:

$$D_{T,i}^{\star} = -2.5 \sum_{j \neq K} D_{ij}^{\star} \sum_k L_{jk}^{00,10} \widetilde{a}_{10,k} \tag{23}$$

$$\lambda = -\frac{4}{\mathcal{K}} \sum_i X_i \left(\widetilde{a}_{10,i} + \frac{X_i}{L_{ii}^{01,01}} - \sum_j F_{ij}^{01,10} \widetilde{a}_{10,j} \right) \tag{24}$$

with

$$\widetilde{a}_{10,i} \approx \sum_{r=0}^{n} w_i^{(r)} \tag{25}$$

$$w_i^{(0)} = \frac{1}{L_{ii}^{10,10}} \left(X_i - \sum_k F_{ki}^{01,10} X_k \right) \tag{26}$$

$$w_i^{(r)} = w_i^{(r-1)} + \frac{1}{L_{ii}^{10,10}} \sum_j \left(-L_{ij}^{10,10} + \mathcal{G}_{ij} + \mathcal{H}_{ij} \right) w_j^{(r-1)} \tag{27}$$

$$\text{with} \quad \mathcal{G}_{ij} = \sum_k \left(\widehat{L}_{ik}^{10,00} \sum_{\ell \neq K} D_{k\ell}^{\star} L_{\ell j}^{00,10} \right)$$

$$\text{and} \quad \mathcal{H}_{ij} = \sum_k L_{ik}^{10,01} F_{kj}^{01,10}$$

In this case, there is no need to invert matrices, other than in order to obtain $D_{ij}^{\star}$ from (19)-(21). Instead, matrix-vector multiplications are performed as summarised in Figure 1 of [16] where, using their notations: $w_i^{(r)} = w_i^{(r-1)} + v_{1,i}^{(r)} + v_{2,i}^{(r)} - v_{5,i}^{(r)}$ with $v_{1,i}^{(r)} = \sum \mathcal{G}_{ij} w_j^{(r-1)} / L_{ii}^{10,10}$, $v_{2,i}^{(r)} = \sum \mathcal{H}_{ij} w_j^{(r-1)} / L_{ii}^{10,10}$ and $v_{5,i}^{(r)} = \sum L_{ij}^{10,10} w_j^{(r-1)} / L_{ii}^{10,10}$.

2.4. Extended $1 + M$ model for the thermodiffusion problem

In order to further reduce the cost of the formulation of Córdoba and Arias-Zugasti [16], we can see that an additional approximation can be made. By taking advantage of the definition of main species (22), we can remove the species considered to be dilute from the sums in (23), (24), (26) and (27).

In (23), we can easily see from B that $L_{jk}^{00,10}$ is negligible if one of the two species j or k is dilute since X_j and X_k are small. In (24), the terms in the sum are directly multiplied by a factor X_i and $F_{ij}^{01,10}$ is negligible if j is dilute, such that the contributions from dilute species can also be neglected. Therefore, it is sufficient to compute the approximation (25) for main species only. In (26), we can again neglect the contributions from dilute species in the sum, and in (27) we can again easily see from B that $L_{ij}^{10,10}$, $L_{ki}^{00,10}$, $L_{\ell j}^{00,10}$, $L_{ki}^{01,10}$ or $F_{kj}^{01,10}$ are negligible if j, k or ℓ are dilute species.

In this way, we obtain an accurate approximation of the solution of (3) by resolving (23)-(27) where only the main species are retained. Note that in this case it is not necessary to evaluate the block matrices $L_{ij}^{00,10}$, $L_{ij}^{10,10}$, $L_{ij}^{01,10}$ and the diagonal matrix $L_{ii}^{01,01}$ for dilute species i and j. Neither do we need to compute binary diffusion coefficients $\mathcal{D}_{ij}$ involving dilute species. The necessary binary diffusion coefficients are already available from the lowest order $1 + M$ model [15] (involving at least one main species), computed from (43).

As in [15], the molecular viscosity μ can be accurately approximated by removing the dilute species from the sums in Wilke semi-empirical formula (modified by Bird *et al.*) [5]:

$$\mu = \sum_k \frac{X_k \eta_k}{\sum_j X_j \Phi_{kj}} \quad \text{with} \quad \Phi_{kj} = \left(1 + \sqrt{\frac{\eta_k}{\eta_j}}\sqrt{\frac{W_j}{W_k}}\right)^2 \Bigg/ \sqrt{8\left(1 + \frac{W_k}{W_j}\right)} \tag{28}$$

where η_k is obtained from (43) for main species only.

3. 1D counterflow diffusion flames

In order to validate the proposed extended $1+M$ model, counterflow diffusion flames are considered.

The 1D solution of the axisymmetric opposed-jet configuration problem is obtained by solving the continuity, momentum, species and temperature equations described in [17, 18]. The equations are implemented in the computer code LFLAM developed at Ciemat, used for instance in [19]. Neglecting radiation effects, the equations can be written on the symmetry axis (axial coordinate x) in their unsteady form as follows (here, with $m = 3$ in the cylindrical geometry):

$$\frac{1}{(m-1)}\frac{\partial \rho}{\partial t} = \rho G - \frac{\partial F}{\partial x}, \tag{29}$$

$$\rho\frac{\partial G}{\partial t} = -(m-1)F\frac{\partial G}{\partial x} + \frac{\partial}{\partial x}\left[\mu\frac{\partial G}{\partial x}\right] + H + m\rho G^2 - (m-1)G\frac{\partial F}{\partial x}, \tag{30}$$

$$\rho\frac{\partial T}{\partial t} = -(m-1)F\frac{\partial T}{\partial x} + \frac{1}{\overline{C_p}}\frac{\partial}{\partial x}\left[\lambda\frac{\partial T}{\partial x}\right] - \frac{1}{\overline{C_p}}\sum h_k\dot{\omega}_k + \frac{1}{\overline{C_p}}\left[\sum C_{p,k}(\rho Y_k V_k)\right]\frac{\partial T}{\partial x}, \tag{31}$$

$$\rho\frac{\partial Y_k}{\partial t} = -(m-1)F\frac{\partial Y_k}{\partial x} + \frac{\partial}{\partial x}\left[-\rho Y_k V_k\right] + \dot{\omega}_k, \tag{32}$$

with $(m-1)F = \rho u$ and $\rho G = -\rho v/r$, where u and v are respectively the axial and radial velocity components and r is the radial coordinate. The thermodynamic coefficients $C_{p,k}$ and h_k (resp. specific heat capacity and enthalpy of species k) are obtained from temperature-dependent polynomial fits (NASA polynomials) [20] and $\overline{C_p}$ is the specific heat capacity of the mixture. The mixture density ρ is obtained from the ideal gas law at the given pressure. The reaction rate $\dot{\omega}_k$ of species k is obtained from a given chemical mechanism, as function of composition vector $\mathbf{Y}$, temperature T and pressure.

The system of equations (29)-(32) is solved in its steady form, using the algorithm "Twopnt program for boundary value problems" [21]. When the unsteady equations are solved in order to obtain transient solutions (as for instance the igniting flamelets considered in the following), the DDASSL solver is used [22]. In both cases, the block tridiagonal Jacobian matrix of the system is written exactly (instead of being evaluated numerically as in most implementations).

Three different formulations for the boundary conditions are considered. The potential flow formulation consists in assuming $\rho G = dF/dx =$ constant at both boundaries (fuel "fu" and oxidiser "ox"), while a fixed stagnation point is specified at the middle of the domain in order to discretise the continuity equation (29). The strain rate a, defined as the velocity gradient du/dx on the oxidiser side, is therefore the parameter that defines the problem, implying: $(m-1)G_{\text{ox}} = -a$, $H = -\rho_{\text{ox}}.G_{\text{ox}}^2$ and $G_{\text{fu}} = G_{\text{ox}}.(\rho_{\text{ox}}/\rho_{\text{fu}})^{1/2}$. In the plug-flow formulation, a fixed velocity u_{fu} is specified at the fuel boundary, implying: $F_{\text{fu}} = \rho_{\text{fu}}u_{\text{fu}}/(m-1)$ and $G_{\text{fu}} = 0$. On the oxidiser boundary the condition $G_{\text{ox}} = 0$ is applied and the value of H is adjusted during the calculation such that the velocity at the oxidiser boundary matches the target velocity u_{ox}. In this case, the location of the stagnation point depends on the values specified for u_{fu} and u_{ox} and on the density profile, and a global strain rate is defined as $a = (2|u_{\text{ox}}|/L)[1 + (|u_{\text{fu}}|/|u_{\text{ox}}|)\sqrt{\rho_{\text{fu}}/\rho_{\text{ox}}}]$, with L the length of the domain. Finally, in the unsteady calculations considered in the following, a mixed boundary condition will be used where the potential flow assumption is applied on the oxidiser side with given strain rate a (with $(m-1)G_{\text{ox}} = -a$ and $H = -\rho_{\text{ox}}.G_{\text{ox}}^2$), and where the velocity u_{fu} is specified on the fuel side (with $F_{\text{fu}} = \rho_{\text{fu}}u_{\text{fu}}/(m-1)$ and $G_{\text{fu}} = 0$). In this case, the location of the stagnation point depends on the values specified for both a and u_{fu}, and may slightly move in time when considering transient solutions depending on the density profile evolution.

The diffusion fluxes $\rho Y_k V_k$ and thermal conductivity λ are obtained either from the standard Dixon-Lewis formulation presented in 2.2, either using the extended $1 + M$ model presented in 2.4. In order to compare computational times, the standard mixture-averaged approximation [23] can also be used to obtain

$\rho Y_k V_k$ (68), together with the mixture-averaged expressions for Fick diffusion coefficients $D_k^{(\mathrm{MA})}$ (70), thermal diffusion coefficients $D_{T,k}^{(\mathrm{MA})}$ for "light" species (71) and thermal conductivity $\lambda^{(\mathrm{MA})}$ (73) given in D. In all cases, the molecular viscosity μ is obtained from (28) where the sums are reduced to the main species only when the extended $1 + M$ model is used.

In order to analyse the results obtained with the different multicomponent transport approximations, we also consider a conserved scalar Z: a non-reactive "mass fraction" equal to 1 in the fuel stream and equal to 0 in the oxidiser stream. The diffusion of this "mixture fraction" is assumed to correspond to Lewis number equal to one, such that we solve the following extra equation:

$$\rho\frac{\partial Z}{\partial t} = -(m-1)F\frac{\partial Z}{\partial x} + \frac{\partial}{\partial x}\left[\frac{\lambda}{\overline{C_p}}\frac{\partial Z}{\partial x}\right], \tag{33}$$

In this way, the solution of (29)-(32) can be considered either in the 1D physical space as $T(x)$ and $Y_k(x)$, either in Z-space as $T(Z)$ and $Y_k(Z)$.

4. Results

Table 1: Conditions of temperature T and species mole fractions X_k of fuel and oxidiser for the different cases considered at atmospheric pressure, together with the chemical mechanisms used in the calculations

	Fuel	Oxidiser	Mech.
Case 1a Cabra *et al.* [24]	$T = 320K$ $X_{CH_4} = 0.33$ $X_{O_2} = 0.15$ $X_{N_2} = 0.52$	$T = 1350K$ $X_{H_2O} = 0.15$ $X_{O_2} = 0.12$ $X_{N_2} = 0.73$	58 species [28]
Case 1b Cabra *et al.* [24]	see Case 1a	see Case 1a	26 species E [29]
Case 2a Dally *et al.* [25]	$T = 300K$ $X_{CH_4} = 0.5$ $X_{H_2} = 0.5$	$T = 300K$ $X_{O_2} = 0.2086$ $X_{N_2} = 0.7914$	58 species [28]
Case 2b Dally *et al.* [25]	see Case 2a	see Case 2a	26 species E [29]
Case 3 Zhou *et al.* [26]	$T = 300K$ $X_{C_2H_4} = 1.0$	$T = 300K$ $X_{O_2} = 0.18$ $X_{N_2} = 0.82$	202 species [30]
Case 4 Stagni *et al.* [27]	$T = 700K$ $X_{C_7H_{16}} = 0.04556$ $X_{O_2} = 0.20043$ $X_{N_2} = 0.75401$	$T = 300K$ $X_{O_2} = 0.21$ $X_{N_2} = 0.79$	300 species [31]

As summarised in Table 1, different 1D counterflow flames at atmospheric pressure are considered in order to validate the accuracy of the extended $1 + M$ model and to evaluate its efficiency. The counterflow diffusion flames in Case 1 and Case 2 correspond to the conditions of experimental methane turbulent jet flames [24, 25], and Case 3 corresponds to an experimental ethylene counterflow diffusion flame [26]. The counterflow flame considered in Case 4 was studied numerically [27]. It includes autoignition, premixed flame propagation and non-premixed combustion since it corresponds to a hot rich premixed mixture of *n*-heptane in air injected on the fuel side.

4.1. Accuracy of the $1 + M$ extended model

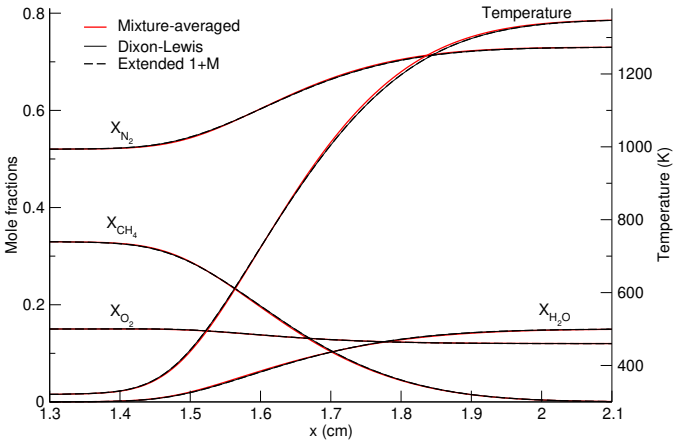

Figure 1: Inert mixing solution corresponding to Case 1a from Table 1 at strain rate $a = 100s^{-1}$ (with fuel boundary at $x = 0$cm, oxidiser boundary at $x = 10$cm and fuel velocity $u_{\mathrm{fu}} = 40$cm/s): mole fraction and temperature profiles.

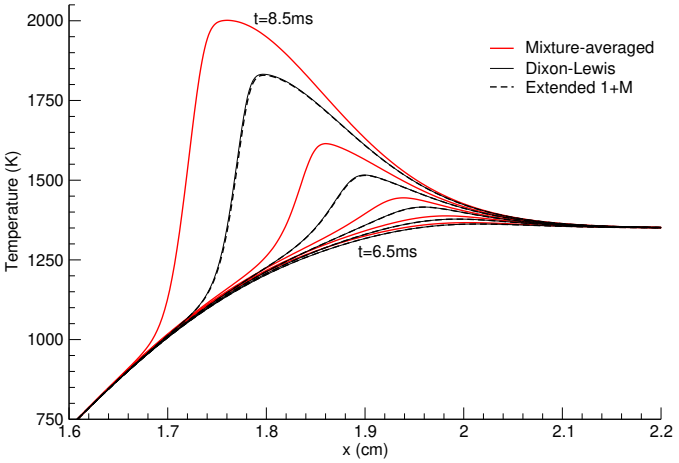

Figure 2: Igniting diluted methane flamelet corresponding to Case 1a from Table 1 at strain rate $a = 100s^{-1}$ (starting from inert solution; with fuel boundary at $x = 0$cm, oxidiser boundary at $x = 10$cm and fuel velocity $u_{\mathrm{fu}} = 40$cm/s). Temperature profiles at discrete times t: every 0.5ms between $t = 6.5$ms and $t = 8.5ms$.

The accuracy of the extended $1 + M$ model can be illustrated by considering autoigniting flamelets starting from inert mixing solutions shown in Figure 1, corresponding to Case 1a in Table 1. In this case, the fuel and oxidiser conditions correspond to the flame experimentally investigated by Cabra *et al.* [24] at atmospheric pressure: a turbulent jet of methane/air mixture in a coflow of hot products of lean premixed hydrogen/air combustion. Figure 2 shows temperature profiles at different times of igniting flamelets. This is a relevant test case in order to evaluate the accuracy of diffusive transport since ignition involves different species in the ignition process like HO_2, H_2O_2, CH_2O

or C_2H_6. We can verify in Figure 2 that the temperature evolution obtained using the extended 1 + M model matches almost exactly the evolution obtained using the standard Dixon-Lewis formulation. On the other hand, we can see in this case how the mixture-averaged approximation leads to large discrepancies in the temperature time evolution of the igniting flamelet. Note that we could verify that these discrepancies are mostly due to the small differences in the initial inert solution shown in Figure 1.

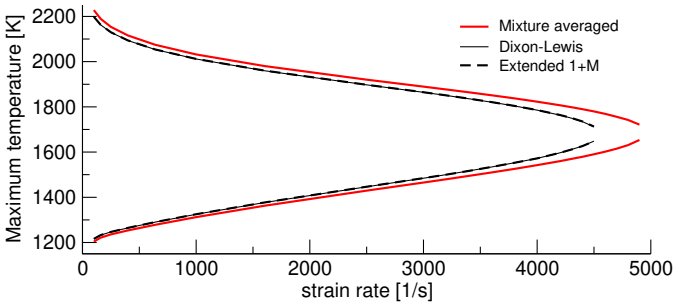

Figure 3: S-curve corresponding to Case 2a from Table 1 (potential flow steady calculations).

A different way to show the accuracy of the extended 1 + M model is to consider the maximum temperature of both stable and unstable steady solutions at different strain rates up to extinction ("S-curve"). Figure 3 shows the S-curve corresponding to the conditions of the Sydney bluff-body stabilised flames [25] (Case 2a in Table 1), where the fuel is a mixture of CH_4 and H_2. We can again observe that the results are almost indistinguishable whether the standard Dixon-Lewis multicomponent formulation or the extended 1 + M model is used. The mixture-averaged approximation predicts different maximum temperatures and leads to extinction at a higher strain rate in this case.

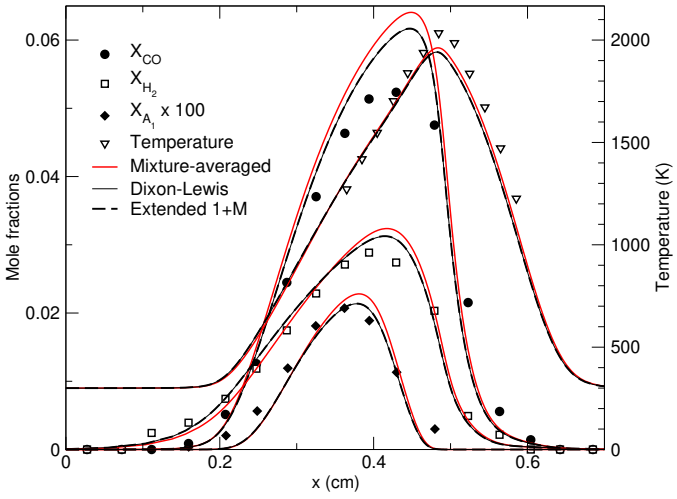

Figure 4: Species mole fraction and temperature profiles corresponding to Case 3 from Table 1 at strain rate $a = 108.61\text{s}^{-1}$ (potential flow steady calculations: the computational results are shifted in x-space in order to compare to experimental data from Zhou *et al.* [26]).

We can also compare in more detail the flame structure by looking at species concentration profiles. We consider here results for the ethylene counterflow flame studied by Zhou *et al.* [26] in their research on soot formation (Case 3 in Table 1). In this case, we use a rather large 202-species hydrocarbon-PAH mechanism including polycyclic aromatic hydrocarbon (PAH) formation [30]. Figure 4 shows profiles of temperature and mole fractions of CO, H_2 and benzene (referred to as A_1), where the formation of the latter is critical for larger PAHs and soot formation. Again, the extended 1 + M model results are identical to standard Dixon-Lewis results, while discrepancies are observed with the mixture-averaged assumption.

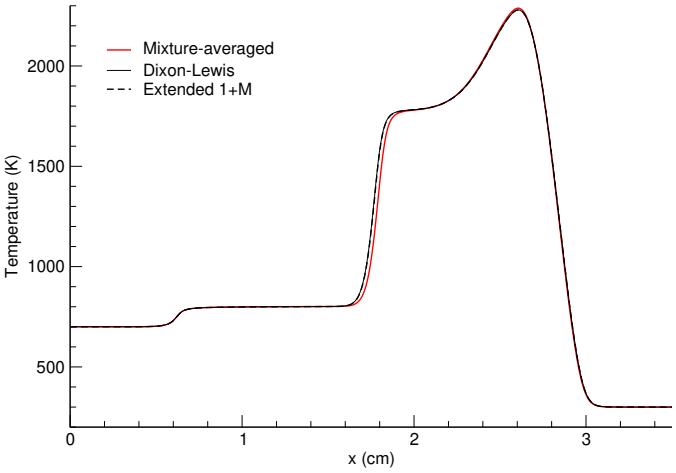

Figure 5: Temperature profiles corresponding to Case 4 from Table 1 at global strain rate $a = 40\text{s}^{-1}$ (plug-flow steady calculations, with fuel velocity 76 cm/s, oxidiser velocity 17.5 cm/s, and domain length 3.5 cm).

In order to deal with an even larger chemical mechanism, Case 4 studied numerically by Stagni *et al.* [27] is also considered, using a large 300-species low temperature oxidation mechanism for n-heptane [31]. At atmospheric pressure, a rich premixed mixture of n-heptane and air at equivalence ratio 2.5 is injected on the fuel side at 700K (temperature where the mixture can autoignite), and air at 300K is injected on the oxidiser side. Figure 5 shows the temperature profile of the corresponding steady flame at global strain rate $a = 40\text{s}^{-1}$. Starting from the fuel boundary we can observe a first low temperature rise corresponding to autoignition of the premixed mixture, a second temperature rise corresponding to flame propagation towards the fuel boundary and a third temperature peak corresponding to the diffusion flame. We can again observe that the extended 1+M model gives the same results as standard Dixon-Lewis, whereas the mixture-averaged approximation appears to predict a lower flame propagation velocity and a slightly higher temperature peak in this case.

In order to consider the efficiency of the extended 1 + M model, we repeat Case 1a and Case 2a with a skeletal mechanism involving 26 species only [29] (resp. Case 1b and Case 2b). The skeletal mechanism was deduced from the 58-species San Diego mechanism [28] used in Case 1a and Case 2a, and is given in E. Case 1b and Case 2b are interesting since practical 3D calculations of methane flames would usually require the use of such reduced mechanisms in order to reduce computational cost. Figures 6 and 7 show that the solutions obtained

with the skeletal mechanism are indeed comparable to the solutions obtained with the detailed mechanism shown in Figures 2 and 3.

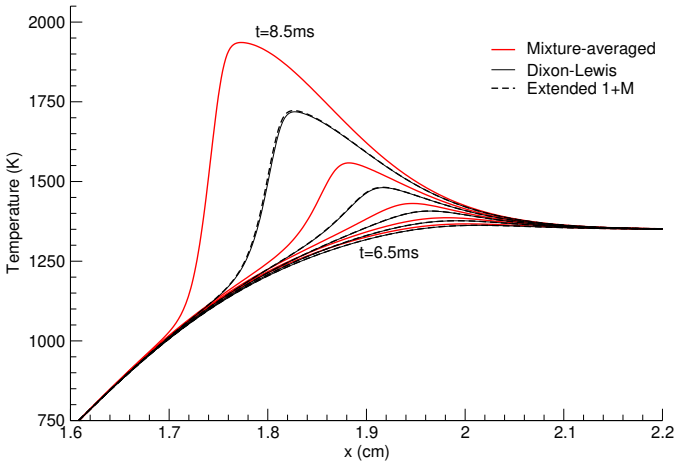

Figure 6: Igniting diluted methane flamelet corresponding to Case 1b from Table 1 (legend: see Figure 2).

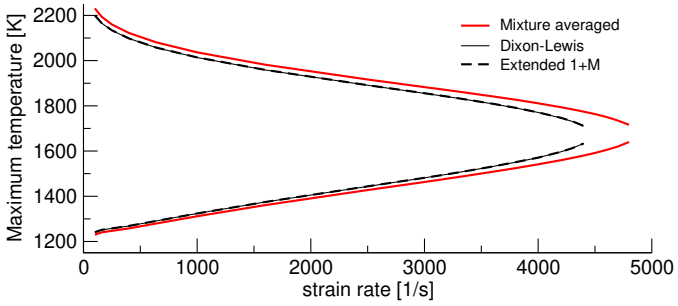

Figure 7: S-curve corresponding to Case 2b from Table 1 (potential flow steady calculations).

4.2. *Cost of diffusion coefficient evaluation*

We consider here the time $\tau_{\text{Fick}} = \tau^{(F)}_{\mathbb{L}} + \tau^{(F)}_{\text{solve}}$ spent on the evaluation of Fick diffusion coefficients and $\tau_{\text{therm}} = \tau^{(T)}_{\mathbb{L}} + \tau^{(T)}_{\text{solve}}$ the time spent on the evaluation of thermal diffusion coefficients and thermal conductivity, where $\tau^{(F)}_{\mathbb{L}}$ is the time spent on the construction of block matrix $\mathbb{L}^{00,00}$ and $\tau^{(T)}_{\mathbb{L}}$ the time spent on the construction of the other blocks of matrix $\mathbb{L}$. The times $\tau^{(F)}_{\text{solve}}$ and $\tau^{(T)}_{\text{solve}}$ correspond to the remaining time spent on the evaluation of the diffusion coefficients (where we do not include the time spent on binary diffusion coefficients evaluation, $\mathcal{D}_{ij}$). In Case 1a and Case 1b, the times are deduced from the steady solutions at the considered strain rate $a = 100\text{s}^{-1}$. In Case 2a and Case 2b, only one strain rate from the stable steady solutions is considered at $a = 100\text{s}^{-1}$. In Case 3 and Case 4, we use the calculations from Figure 4 and 5.

First of all, we verify the scaling of the times $\tau^{(F)}_{\text{solve}}$ and $\tau^{(T)}_{\text{solve}}$. When using the standard Dixon-Lewis formulation, $\tau^{(F)}_{\text{solve}}$ is mostly the time spent on the inversion of $\mathbb{L}^{00,00}$ which should scale as $N^3_* = N^3$, whereas when using the extended $1 + M$ model, it is the sum of the time $\tau^{(F)}_{11}$ spent on the inversion of the $M \times M$ matrix of main species in (19) which should scale as $N^3_* = \left\langle M^3 \right\rangle$ and the time $\tau^{(F)}_{12}$ spent on the block matrix multiplication in (20) which should scale as $N^3_* = \left\langle M^2(N - M - 1) \right\rangle$. Here, the brackets refer to the average value over the 1D domain: for instance $\left\langle M^3 \right\rangle$ is the average value of the cube of the number of main species M.

The time $\tau^{(T)}_{\text{solve}}$ mostly corresponds to the resolution of $\mathcal{K}\mathbb{L}.\mathbf{a} = \mathbf{X}$, such that it should scale as $N^3_* = (3N - n^\star)^3$ when using Dixon-Lewis. When using the Neuman series approximation (25)-(27), it should scale as $N^2_* = (3N - n^\star - 1)^2$ with the approximation of Córdoba and Arias-Zugasti [16], and $N^2_* = \left\langle (3\mathcal{N}_M - n^\star_M - 1)^2 \right\rangle$ with the extended $1+M$ model, where $n^\star_M$ is the number of monatomic main species.

In order to compare times from the different cases, we nondimensionalise the times by an average computational time spent on one single chemical reaction:

$$\overline{\tau}_{\text{prop}} = \frac{\tau_{\text{prop}}}{\tau_{\text{chem}}/N_{\text{reac}}} \tag{34}$$

where τ_{chem} is the time spent on the evaluation of the chemical source terms $\dot{\omega}_k$ and N_{reac} is the number of reactions in the chemical mechanism considered, such that $\tau_{\text{chem}}/N_{\text{reac}}$ is the averaged time spent on one single reaction and has similar values for the different test cases (and different chemical mechanisms) considered.

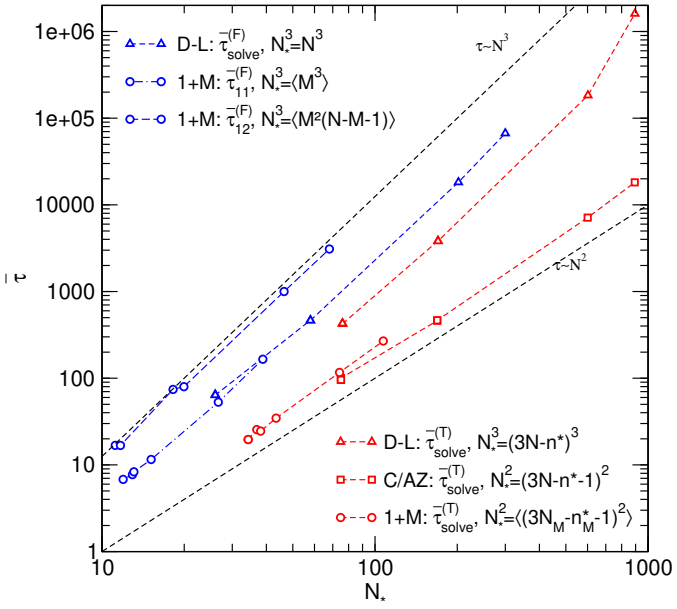

Figure 8: Dimensionless times from (34) spent on Fick (blue) and thermodiffusion (red) problem resolution, as function of N_* defined for each curve (see legend in the figure): using Dixon-Lewis standard formulation (D-L), Córdoba and Arias-Zugasti approximation (C/AZ) and the extended $1+M$ model (1+M).

Figure 8 illustrates the scaling of $\overline{\tau}^{(F)}_{\text{solve}}$ (where $\overline{\tau}^{(F)}_{\text{solve}} = \overline{\tau}^{(F)}_{11} + \overline{\tau}^{(F)}_{12}$, with the extended $1 + M$ model) and $\overline{\tau}^{(T)}_{\text{solve}}$ as function of N_* as discussed above. Concerning Fick diffusion coefficients, we will see more clearly in Figure 9 how the extended $1 + M$ model reduces the time $\overline{\tau}^{(F)}_{\text{solve}}$, compared to Dixon-Lewis. When

using the extended $1 + M$ model we can see that the main contribution to $\overline{\tau}^{(F)}_{\text{solve}}$ is the time $\tau^{(F)}_{12}$ spent on matrix multiplication (20). Concerning the thermodiffusion problem, we clearly see how the approximation of Córdoba and Arias-Zugasti reduces the cost of the resolution of $\mathcal{K}\mathbb{L}.\mathbf{a} = \mathbf{X}$, and how it scales as N^2 as discussed in [16]. Moreover, we can observe the advantage of using the extended $1 + M$ model which further reduces the cost by reducing the size of the problem.

Cost of the construction of matrix $\mathbb{L}$. The computational time $\tau^{(F)}_{\mathbb{L}}$ required for the construction of the first block $\mathbb{L}^{00,00}$ is included in the time τ_{Fick} spent on evaluating the Fick diffusion coefficients, and the time $\tau^{(T)}_{\mathbb{L}}$ for the construction of the remaining blocks of matrix $\mathbb{L}$ is included in the time τ_{therm} spent on thermal diffusion coefficients and thermal conductivity. Times $\tau^{(F)}_{\mathbb{L}}$ and $\tau^{(F)}_{\text{solve}}$ are shown in Figure 9, and times $\tau^{(T)}_{\mathbb{L}}$ and $\tau^{(T)}_{\text{solve}}$ are shown in Figure 10. They are now plotted as a function of the total number of species N in order to compare their values when using different formulations.

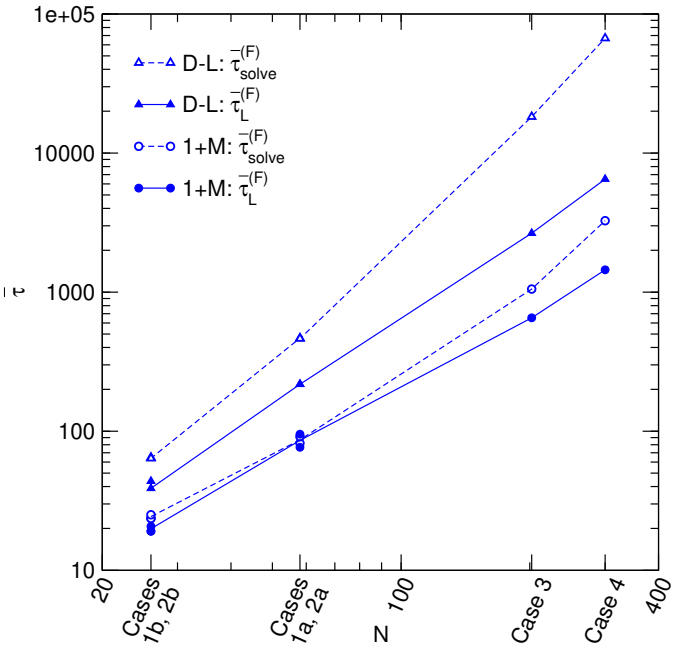

Figure 9: Dimensionless time from (34) $\overline{\tau}_{\text{Fick}} = \overline{\tau}^{(F)}_{\mathbb{L}} + \overline{\tau}^{(F)}_{\text{solve}}$ spent on Fick diffusion coefficient evaluation, as function of the total number of species N, using Dixon-Lewis standard formulation (D-L), and the extended $1 + M$ model (1+M).

We can observe in Figure 9 that when using Dixon-Lewis, the time spent on the inversion of the first block matrix is always larger than the time spent on the construction of $\mathbb{L}^{00,00}$. As mentioned earlier, $\tau^{(F)}_{\text{solve}}$ is significantly reduced when using the extended $1 + M$ model. However, in this case it remains of the same order of magnitude as $\tau^{(F)}_{\mathbb{L}}$, since it is mainly controlled by the time $\tau^{(F)}_{12}$ spent on matrix multiplication (20).

In the same way, we can observe in Figure 10 that with Dixon-Lewis the time spent on the resolution of $\mathcal{K}\mathbb{L}.\mathbf{a} = \mathbf{X}$ is always larger than the time spent on the construction of $\mathbb{L}$. We can observe the gain implied by using the approximation of

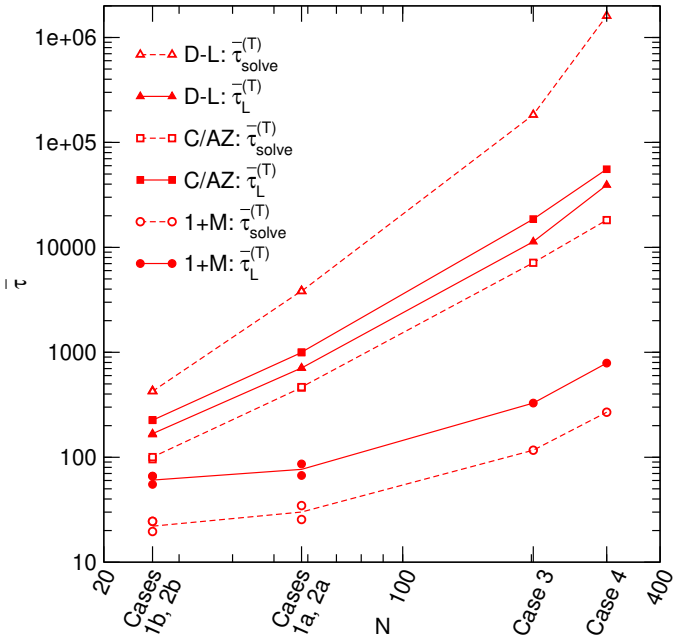

Figure 10: Dimensionless time from (34) $\overline{\tau}_{\text{therm}} = \overline{\tau}^{(T)}_{\mathbb{L}} + \overline{\tau}^{(T)}_{\text{solve}}$ spent on thermodiffusion coefficient evaluation, as function of the total number of species N, using Dixon-Lewis standard formulation (D-L), Córdoba and Arias-Zugasti approximation (C/AZ) and the extended $1 + M$ model (1+M).

Córdoba and Arias-Zugasti (here with $n = 3$ in (25)), where the cost of the resolution of $\mathcal{K}\mathbb{L}.\mathbf{a} = \mathbf{X}$ is now lower than the cost of the construction of $\mathbb{L}$, but of the same order of magnitude. With the extended $1 + M$ model, the cost of the resolution of the system drops dramatically such that the time for the evaluation of thermal diffusion coefficients and thermal conductivity is mostly controlled by the time spent on the construction of $\mathbb{L}$, which is also largely reduced compared to the approximation of Córdoba and Arias-Zugasti.

4.3. Comparison of property evaluation times

We can now compare the global time spent on transport property evaluation which, in addition to τ_{Fick} and τ_{therm}, should also include the time spent on the evaluation of binary diffusion coefficients $\mathcal{D}_{ij}$ from (43) and molecular viscosity μ from (28). In each case, we compute the time τ_{prop} spent on the evaluation of the different properties:

τ_{visc}	viscosity μ
τ_{bdiff}	binary diffusion coefficients $\mathcal{D}_{ij}$
τ_{Fick}	Fick diffusion coefficients D_{ij}
τ_{therm}	thermal diffusion coeff. $D_{T,i}$ and conductivity λ
τ_{chem}	chemical source terms $\dot{\omega}_k$

and we compare the dimensionless times:

$$\widetilde{\tau}_{\text{prop}} = \frac{\tau_{\text{prop}}}{\tau_{\text{chem}}} \tag{35}$$

giving the relative time spent on a given property compared to the time spent on chemical source terms evaluation.

Focusing on the comparison between standard Dixon-Lewis formulation, extended $1 + M$ model and mixture-averaged approximation, all dimensionless times are reported in Table 2 (Case 1b and Case 2b using the 26-species skeletal mechanism), Table 3 (Case 1a and Case 2a using the 58-species mechanism), Table 4 (Case 3 using the 202-species mechanism) and Table 5 (Case 4 using the 300-species mechanism)

Table 2: Dimensionless times from steady flamelet calculations (26-species skeletal mechanism), and average number of main species $\langle \mathcal{N}_M \rangle = \langle 1 + M \rangle$ and maximum number of main species $\mathcal{N}_{M,\max}$ in the computational domain.

$N = 26$	D.-L. Case 1b/2b	$1 + M$ Case 1b	$1 + M$ Case 2b	Mix.-av. Case 1b/2b
$\langle \mathcal{N}_M \rangle$		12.31	10.97	
$\mathcal{N}_{M,\max}$		19	19	
$\widetilde{\tau}_{\text{visc}}$	0.31	0.16	0.14	0.31
$\widetilde{\tau}_{\text{bdiff}}$	0.28	0.24	0.23	0.28
$\widetilde{\tau}_{\text{Fick}}$	1.23	0.50	0.46	0.05
$\widetilde{\tau}_{\text{therm}}$	7.25	1.08	0.93	0.02
Total	9.07	1.98	1.76	0.66

Table 3: Dimensionless times from steady flamelet calculations (58-species mechanism), and average number of main species $\langle \mathcal{N}_M \rangle = \langle 1 + M \rangle$ and maximum number of main species $\mathcal{N}_{M,\max}$ in the computational domain.

$N = 58$	D.-L. Case 1a/2a	$1 + M$ Case 1a	$1 + M$ Case 2a	Mix.-av. Case 1a/2a
$\langle \mathcal{N}_M \rangle$		13.65	11.62	
$\mathcal{N}_{M,\max}$		22	21	
$\widetilde{\tau}_{\text{visc}}$	0.41	0.06	0.04	0.41
$\widetilde{\tau}_{\text{bdiff}}$	0.37	0.28	0.27	0.37
$\widetilde{\tau}_{\text{Fick}}$	2.41	0.48	0.43	0.08
$\widetilde{\tau}_{\text{therm}}$	16.56	0.43	0.34	0.02
Total	19.75	1.25	1.08	0.88

Table 4: Dimensionless times from steady flamelet calculations in Case 3 (202-species mechanism), and average number of main species $\langle \mathcal{N}_M \rangle = \langle 1 + M \rangle$ and maximum number of main species $\mathcal{N}_{M,\max}$ in the computational domain.

$N = 202$	D.-L.	$1 + M$	Mix.-av.
$\langle \mathcal{N}_M \rangle$		21.93	
$\mathcal{N}_{M,\max}$		43	
$\widetilde{\tau}_{\text{visc}}$	1.12	0.04	1.12
$\widetilde{\tau}_{\text{bdiff}}$	0.95	0.60	0.95
$\widetilde{\tau}_{\text{Fick}}$	15.47	0.97	0.20
$\widetilde{\tau}_{\text{therm}}$	144.42	0.33	0.01
Total	161.96	1.94	2.28

We can now quantify more clearly the gain implied by the extended $1+M$ model compared to standard Dixon-Lewis, already observed in Figures 9 and 10. Compared to standard Dixon-Lewis, the extended $1 + M$ model reduces the time $\widetilde{\tau}_{\text{Fick}}$ by a factor 2.5 in the 26-species case up to nearly a factor 20 in the 300-species case, and it reduces the time $\widetilde{\tau}_{\text{therm}}$ by a factor 7 in the 26-species case up to a factor 1500 in the 300-species case.

Table 5: Dimensionless times from steady flamelet calculations in Case 4 (300-species mechanism), and average number of main species $\langle \mathcal{N}_M \rangle = \langle 1 + M \rangle$ and maximum number of main species $\mathcal{N}_{M,\max}$ in the computational domain.

$N = 300$	D.-L.	$1 + M$	Mix.-av.
$\langle \mathcal{N}_M \rangle$		31.06	
$\mathcal{N}_{M,\max}$		63	
$\widetilde{\tau}_{\text{visc}}$	0.33	0.01	0.33
$\widetilde{\tau}_{\text{bdiff}}$	0.30	0.17	0.30
$\widetilde{\tau}_{\text{Fick}}$	6.25	0.33	0.06
$\widetilde{\tau}_{\text{therm}}$	139.01	0.09	0.002
Total	145.89	0.60	0.69

When using the extended $1+M$ model, also thanks to the gain on molecular viscosity evaluation, the total time spent on transport property evaluation is of the same order as the mixture-averaged time (and of the same order as the time τ_{chem} spent on chemical source term evaluation). The total time with the extended $1 + M$ model is even smaller than mixture-averaged for large number of species N. Compared to standard Dixon-Lewis formulation, the total time is already reduced by a factor 5 when using the 26-species mechanism, and drops as the number of species considered increases: by a factor 15 with 58 species, by a factor 85 with 202 species and by a factor 240 with 300 species.

As reflected in Table 2 and Table 3, when using Dixon-Lewis formulation or mixture-averaged approximation, the dimensionless times only depend on the chemical mechanism used and not on the test case considered, since the evaluation of properties depends on the number of species N. When using the extended $1+M$ model, for a given chemical mechanism, the average number of main species $\langle \mathcal{N}_M \rangle = \langle 1 + M \rangle$ depends on the case considered and the dimensionless times are shorter as $\langle \mathcal{N}_M \rangle$ is lower.

4.4. Main species distribution

The efficiency of the extended $1 + M$ model is closely related to the average number of main species $\langle \mathcal{N}_M \rangle = \langle 1 + M \rangle$. It is therefore useful to look at the distribution of the number of main species $\mathcal{N}_M = 1 + M$ in the different calculations.

Figures 11, 12 and 13 show the distributions of the number of main species corresponding to the counterflow diffusion flame calculations reported in Tables 3 and 4, both in physical space x and as a function of the "mixture fraction" Z corresponding to (33). The temperature profiles also give an idea on the discretisation of the 1D domain by showing the distribution of grid points (symbols).

In all three cases, we can observe how the number of main species reduces to the few species given as boundary conditions in Table 1 in pure fuel and pure oxidiser. In 3D calculations of diffusion flames this will be important since part of the computational cells will indeed correspond to these compositions (in

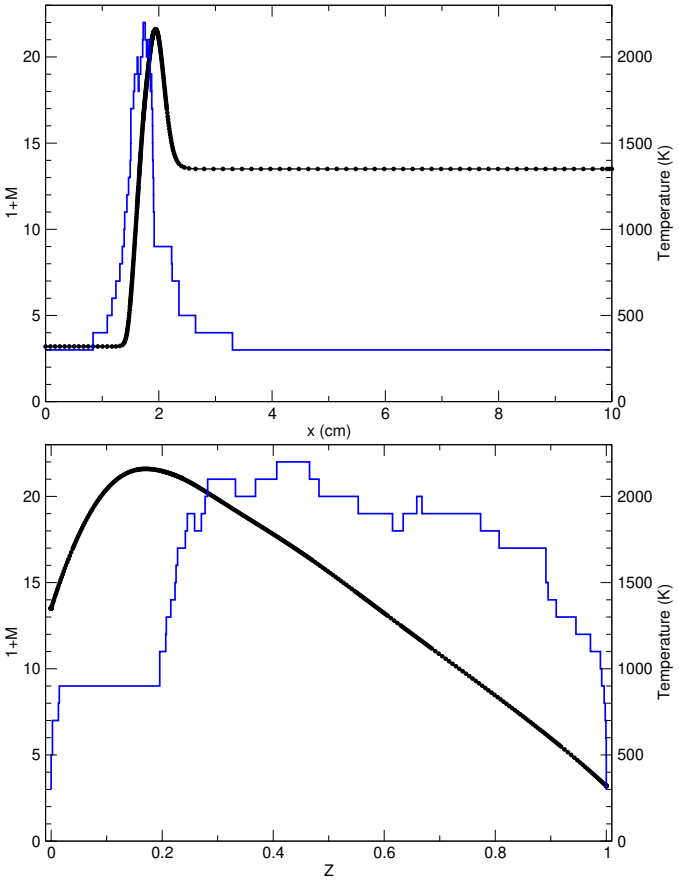

Figure 11: Case 1a corresponding to the calculation reported in Table 3 (steady flamelet at strain rate $a = 100\text{s}^{-1}$, with plug-flow boundary at $x = 0$cm and potential flow boundary at $x = 10$cm): number of main species $\mathcal{N}_M = 1 + M$ (blue line) and temperature profile (black line and symbols), in 1D physical space (top) and as a function of Z from (33) (bottom).

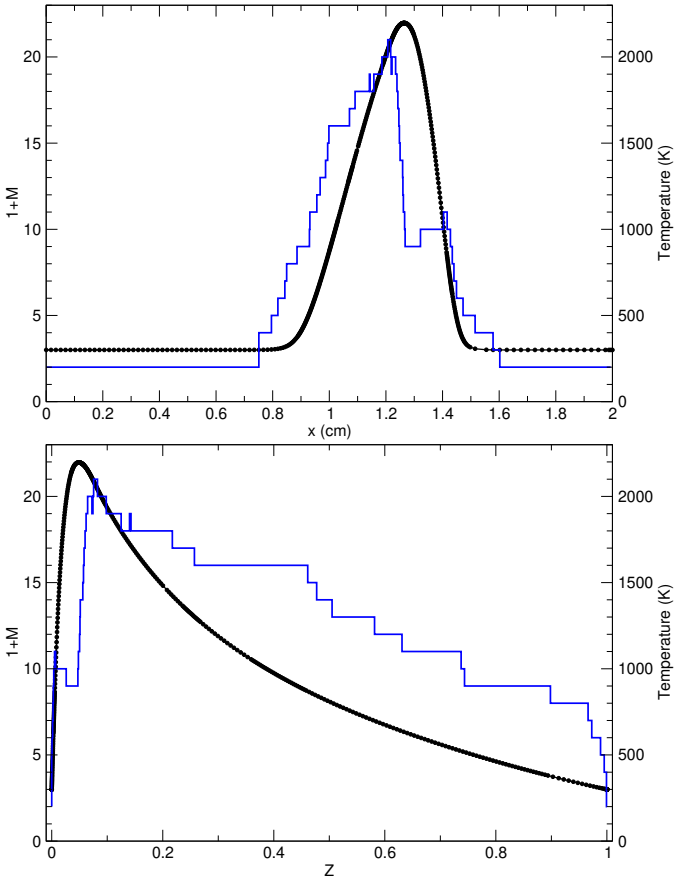

Figure 12: Case 2a corresponding to the calculation reported in Table 3 (steady flamelet at strain rate $a = 100\text{s}^{-1}$ with potential flow boundaries both at $x = 0$cm and $x = 2$cm): see caption from Figure 11.

particular pure oxidiser corresponding to the coflow composition in jet flame configurations).

Another observation in all three cases is that the number of main species is the highest on the rich side of the flame. This corresponds to the mixing between combustion products on the rich side of the reaction zone and pure fuel mixture. We can expect that this will imply a high efficiency of the extended $1 + M$ model in 3D calculations of realistic diffusion flames where the oxidiser is usually in excess and where a large part of the computational domain therefore corresponds to lean mixtures.

In Figures 14, the distribution of the number of main species corresponding to the partially premixed counterflow flame calculation reported in Table 5 is shown in physical space (in this partially premixed case, a representation in Z-space would not make much sense). It is interesting to observe how the number of main species is the highest in the autoignition zone, in the following "cool flame" region and in the premixed flame propagation front. We can again expect that in realistic 3D calculations of n-heptane spray flames corresponding to these conditions, the region of large number of main species would correspond to a reduced part of the total computational domain.

5. Conclusions

An accurate and efficient multicomponent transport model for both Fick diffusion fluxes and thermal diffusion fluxes has been presented. It combines the lowest order $1 + M$ model formulation by Naud and Arias-Zugasti [15] for the evaluation of Fick diffusion coefficients (including an efficient approximation of molecular viscosity) and an extension of the recent formulation by Córdoba and Arias-Zugasti [16] for the evaluation of thermal diffusion coefficients and thermal conductivity. We show that the dimension of the latter can indeed be significantly reduced by removing all the species considered dilute according to the $1 + M$ formulation by Naud and Arias-Zugasti.

Different calculations of steady and unsteady 1D counterflow flames are performed. The proposed extended $1 + M$ model results prove to be in almost perfect correpondence with the results from the complete Dixon-Lewis formulation. The total cost of the extended $1+M$ model appears to be of the same order as the standard mixture-averaged model in all cases, being even cheaper when the number of species N is large.

Concerning Fick diffusion coefficients, we show how the efficient $1 + M$ model by Naud and Arias-Zugasti reduces both the cost of the construction and the evaluation of the inverse of matrix $\mathbb{L}^{00,00}$, compared to standard Dixon-Lewis formulation. The time spent on the matrix inverse is similar to the time spent

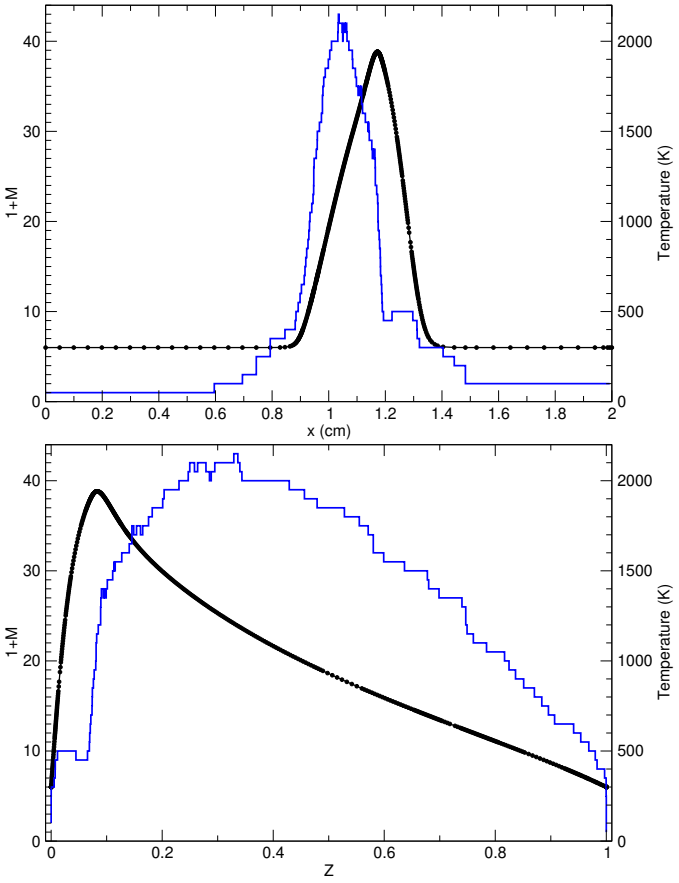

Figure 13: Case 3 corresponding to the calculation reported in Table 4 (steady flamelet at strain rate $a = 108.61\text{s}^{-1}$ with potential flow boundaries both at $x = 0$cm and $x = 2$cm): see caption from Figure 11.

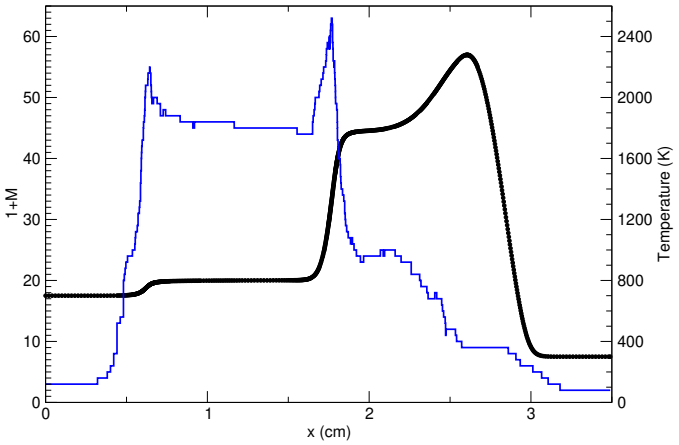

Figure 14: Case 4 corresponding to the calculation reported in Table 5 (steady flamelet at global strain rate $a = 40\text{s}^{-1}$ with plug flow boundaries both at $x = 0$cm and $x = 3.5$cm): see caption from Figure 11 (here only in physical space).

on the construction of the matrix. It is mostly controlled by the diffusion of main species into dilute species (20), compared to the $M \times M$ matrix inversion concerning main species only. Compared to standard Dixon-Lewis, this leads to a reduction by a factor 2.5 in the 26-species case up to nearly a factor 20 in the 300-species case.

Concerning the thermodiffusion problem, we verify that the recent formulation by Córdoba and Arias-Zugasti implies a significant cost reduction compared to standard Dixon-Lewis formulation. It is mostly related to the reduction of the cost of the resolution of the system $\mathcal{K}\mathbb{L}.\mathbf{a} = \mathbf{X}$, which becomes similar to the cost of the construction of matrix $\mathbb{L}$. With the proposed extended $1 + M$ model, the cost is further reduced due to the reduction of the size of the problem. Compared to standard Dixon-Lewis, this leads to a reduction by a factor 7 in the 26-species case up to a factor 1500 in the 300-species case.

With the extended $1 + M$ model, the total cost of transport coefficient evaluation (Fick and thermal diffusion coefficients, thermal conductivity, molecular viscosity) is reduced by a factor 5 when using a rather small 26-species skeletal mechanism for methane oxidation. It is reduced by an order of magnitude when a detailed 58-species mechanism is used, and by two orders of magnitude with a 202-species or a 300-species mechanism.

For the counterflow diffusion flames considered, we show that the number of main species considered in the extended $1 + M$ model is the highest for rich mixtures. This suggests that the proposed model will be very efficient in realistic diffusion flame calculations where a large part of the computational domain will correspond to lean mixtures, and where a significant part of the computational domain will even possibly correspond to pure oxidiser composition. The distribution of main species in the more complex case of a partially premixed rich n-heptane/air counterflow diffusion flame (including autoignition) also suggests that the proposed model would be very efficient in realistic 3D calculations of n-heptane sprays.

Acknowledgments

This work is supported by the Spanish Research Agency, at Ciemat under project #PID2019-108592RB-C42/AEI/10.13039/501100011033, and at UNED (Madrid) under project #PID2019-108592RB-C44/AEI/10.13039/501100011033. At UNED, this work is also partially supported by European Regional Development Funds (ERDF). The authors also acknowledge Ciemat and UNED funding for open access publishing.

A. Transport properties

In this Appendix, we detail the multicomponent transport properties as implemented in [5].

A.1. Molecular viscosity and binary diffusion coefficients

The single-component viscosity of species k is given as:

$$\eta_k = 2.6693.10^{-5} \frac{\sqrt{TW_k}}{\sigma_k^2 \Omega_{kk}^{(2,2)*}} \tag{36}$$

with W_k the molar weight of molecule k, T the temperature in K and σ_k the Lennard-Jones collision diameter in Å. The binary

diffusion coefficients $\mathcal{D}_{ij}$ in [cm^2/s] are given as:

$$\mathcal{D}_{ij} = 0.001858 \frac{\sqrt{T^3 \frac{W_i+W_j}{W_i W_j}}}{p\sigma_{ij}^2 \Omega_{ij}^{(1,1)*}} \left(1 + \Delta_{ij}\right) \tag{37}$$

with p the pressure in atm and where σ_{ij} is obtained as:

$$\begin{aligned} \sigma_{ij} =& \frac{1}{2}\left(\sigma_i + \sigma_j\right) \text{ if both } i \text{ and } j \text{ are polar or non-polar} \\ \sigma_{ij} =& \frac{1}{2}\left(\sigma_i + \sigma_j\right)\xi^{-1/6} \text{ otherwise} \end{aligned} \tag{38}$$

and where Δ_{ij} is the correction term proposed by Marrero and Mason [33].

The reduced collision integrals $\Omega_{ij}^{(1,1)*}$ and $\Omega_{ij}^{(2,2)*}$ are obtained from quadratic interpolations of the tables based on Stockmayer potentials given in Monchick and Mason [1], as functions of the reduced temperatures T_{ij}^* and reduced dipole moments δ_{ij}^*:

$$T_{ij}^* = \frac{k_B T}{\epsilon_{ij}} \tag{39}$$

where k_B is the Boltzmann constant and

$$\begin{aligned} \delta_{ij}^* =& \frac{1}{2}\frac{\mu_i \mu_j}{\sqrt{\epsilon_{ij}}\sigma_{ij}^3} \text{ if both } i \text{ and } j \text{ are polar or non-polar} \\ \delta_{ij}^* =& 0 \text{ otherwise} \end{aligned} \tag{40}$$

with μ_k the dipole moment of molecule k and where ϵ_{ij} is obtained from the Lennard-Jones potentials ϵ_k:

$$\begin{aligned} \epsilon_{ij} =& \sqrt{\epsilon_i \epsilon_j} \text{ if both } i \text{ and } j \text{ are polar or non-polar} \\ \epsilon_{ij} =& \xi^2 \sqrt{\epsilon_i \epsilon_j} \text{ otherwise} \end{aligned} \tag{41}$$

In the case of a polar molecule p interacting with a non-polar molecule n, the parameter ξ in (38) and (41) reads:

$$\xi = 1 + \frac{1}{4}\frac{\alpha_n}{\sigma_n^3}\frac{\mu_p^2}{\epsilon_p \sigma_p^3}\sqrt{\frac{\epsilon_p}{\epsilon_n}} \tag{42}$$

with α_n the polarizability of the non-polar molecule.

In our practical applications, Equations (36) and (37) are computed over a given range of temperatures $[T_{\min}, T_{\max}]$, and a polynomial fit algorithm is used in order to obtain an approximation of the logarithm of the properties versus the logarithm of the temperature, as:

$$\begin{aligned} \ln \eta_k &= \sum_{n=1}^{4} a_{n,k} \left(\ln T\right)^{n-1} \\ \ln \mathcal{D}_{ij} &= \sum_{n=1}^{4} d_{n,ij} \left(\ln T\right)^{n-1} \end{aligned} \tag{43}$$

such that (36) and (37) are only calculated once over the temperature range $[T_{\min}, T_{\max}]$ at the begin of the calculation in order to evaluate the coefficients $a_{n,k}$ and $d_{n,ij}$. During the calculation, the less time consuming polynomial fits (43) are used in order to evaluate the transport properties.

A.2. Properties required for thermal diffusion

In order to obtain thermal diffusion coefficients and thermal conductivity, the following properties are required:

$$\begin{aligned} C_{v,k} = C_{p,k} - R =& C_{v,k}^{\text{trans}} + C_{v,k}^{\text{int}} \\ =& \underbrace{C_{v,k}^{\text{trans}}}_{C_{v,k}^{\text{trans}} = \frac{3}{2}R} + C_{v,k}^{\text{rot}} + C_{v,k}^{\text{vib}} \end{aligned} \tag{44}$$

where $C_{p,k}$ is the heat capacity at constant pressure of species k and R is the universal gas constant. For monatomic molecules $C_{v,k}^{\text{rot}} = 0$ and $C_{v,k}^{\text{vib}} = 0$, and otherwise:

$$\begin{aligned} \frac{C_{v,k}^{\text{rot}}}{R} &= 1 \quad \text{for linear nolecules} \\ \frac{C_{v,k}^{\text{rot}}}{R} &= \frac{3}{2} \quad \text{for nonlinear nolecules} \end{aligned} \tag{45}$$

Dimensionless matrices A_{ij}^*, B_{ij}^* and C_{ij}^* define the ratios of collision integrals:

$$A_{ij}^* = \frac{1}{2}\frac{\Omega_{ij}^{(2,2)}}{\Omega_{ij}^{(1,1)}},\ B_{ij}^* = \frac{1}{3}\frac{5\Omega_{ij}^{(1,2)} - \Omega_{ij}^{(1,3)}}{\Omega_{ij}^{(1,1)}},\ C_{ij}^* = \frac{1}{3}\frac{\Omega_{ij}^{(1,2)}}{\Omega_{ij}^{(1,1)}} \tag{46}$$

They are tabulated as polynomial functions of $\ln\left(T_{ij}^*\right)$ [1, 5], with T_{ij}^* the reduced temperature defined in (39).

The rotational relaxation collision number ξ_k at temperature T is obtained from its given value at 298K, following the temperature dependence $F(T)$ given by Parker [34] and Brau and Jonkman [35]:

$$\xi_k(T) = \xi_k(298)\frac{F(298)}{F(T)} \tag{47}$$

B. Multicomponent thermodiffusion matrices

Following Dixon-Lewis [4], the multicomponent thermodiffusion problem is written as:

$$\mathcal{K}\begin{pmatrix} \mathbb{L}^{00,00} & \mathbb{L}^{00,10} & \mathbb{0} \\ \mathbb{L}^{10,00} & \mathbb{L}^{10,10} & \mathbb{L}^{10,01} \\ \mathbb{0} & \mathbb{L}^{01,10} & \mathbb{L}^{01,01} \end{pmatrix}\begin{pmatrix} \mathbf{a}_{00} \\ \mathbf{a}_{10} \\ \mathbf{a}_{01} \end{pmatrix} = \begin{pmatrix} \mathbf{0} \\ \mathbf{X} \\ \mathbf{X} \end{pmatrix}, \quad \mathcal{K} = \frac{16T}{25p} \tag{48}$$

with T the temperature, p the pressure, X_k the mole fraction of species k, W_k the molar weight of species k and $\mathcal{D}_{ij}$ the binary diffusion coefficients obtained from (43).

$$\begin{aligned} L_{ij}^{00,00} =& \left[\frac{X_i X_j}{\mathcal{D}_{ij}} - \sum_{k=1}^{N}\frac{X_i X_k}{\mathcal{D}_{ik}}\delta_{ij} + \sum_{k\neq i}^{N}\frac{W_j}{W_i}\frac{X_j X_k}{\mathcal{D}_{ik}}\right] \\ L_{ij}^{00,10} =& -\frac{X_i X_j}{\mathcal{D}_{ij}}\frac{W_i}{W_i + W_j}\left(3C_{ji}^* - \frac{5}{2}\right) \\ & + \sum_{k=1}^{N}\frac{X_i X_k}{\mathcal{D}_{ik}}\frac{W_k}{W_i + W_k}\left(3C_{ik}^* - \frac{5}{2}\right)\delta_{ij} \\ L_{ij}^{10,00} =& L_{ji}^{00,10} \end{aligned}$$

$$
\begin{aligned}
L_{ij}^{10,10} =& \frac{X_i X_j}{\mathcal{D}_{ij}} \frac{W_i W_j}{\left(W_i + W_j\right)^2} \left[\frac{15}{2} + \frac{25}{4} - 3B_{ij}^* \right. \\
& \left. -4A_{ij}^* \left(1 + \frac{5}{3\pi} \left(\frac{c_{rot,i}}{k_B \xi_i} + \frac{c_{rot,j}}{k_B \xi_j} \right) \right) \right] \\
& - \sum_{k=1}^{N} \frac{X_i X_k}{\mathcal{D}_{ik}} \frac{1}{(W_i + W_k)^2} \left[\frac{15}{2} W_i^2 + \left(\frac{25}{4} - 3B_{ij}^* \right) W_k^2 \right. \\
& \left. +4A_{ik}^* \left(1 + \frac{5}{3\pi} \left(\frac{c_{rot,i}}{k_B \xi_i} + \frac{c_{rot,k}}{k_B \xi_k} \right) \right) W_i W_k \right] \delta_{ij} \\
L_{ij}^{10,01} =& \frac{10}{\pi} \left[\frac{X_i X_j}{\mathcal{D}_{ij}} \frac{W_j}{W_i + W_j} A_{ji}^* \frac{c_{rot,j}}{k_B \xi_j} \frac{k_B}{c_{int,j}} \right. \\
& \left. + \sum_{k=1}^{N} \frac{X_i X_k}{\mathcal{D}_{ik}} \frac{W_i}{W_i + W_k} A_{ik}^* \frac{c_{rot,i}}{k_B \xi_i} \frac{k_B}{c_{int,i}} \delta_{ij} \right] \\
L_{ij}^{01,10} =& L_{ji}^{10,01} \\
L_{ij}^{01,01} =& -\frac{25}{4} \frac{k_B}{c_{int,i}} \\
& \times \left(\sum_{k=1}^{N} \frac{X_i X_k}{\mathcal{D}_{ik}} \left(\frac{\mathcal{D}_{ik}}{\mathcal{D}_{ik}^{int}} + \frac{12}{5\pi} \frac{W_i}{W_k} A_{ik}^* \frac{c_{rot,i}}{k_B \xi_i} \frac{k_B}{c_{int,i}} \right) \right) \delta_{ij}
\end{aligned}
$$

As already mentioned after Equation (46), the dimensionless matrices A_{ij}^*, B_{ij}^* and C_{ij}^* are tabulated as polynomial functions. For non-polar gases the binary diffusion coefficients for internal energy $\mathcal{D}_{ik}^{int}$ are approximated by $\mathcal{D}_{ik}$. In the case of collisions between polar molecules of the same species p where the exchange is energetically resonant, a large correction is included of the form discussed by Mason and Monchick [2], as explained by Dixon-Lewis [4, 5]:

$$
\frac{\mathcal{D}_{pp}}{\mathcal{D}_{pp}^{int}} = 1 + \delta_{pp}^{'} \quad \text{with} \quad \delta_{pp}^{'} = \frac{2985}{\sqrt{T^3}} \tag{49}
$$

The rotational and internal parts of the species molecular heat capacities represented by $c_{rot,k}$ and $c_{int,k}$ correspond to:

$$
\begin{aligned}
\frac{c_{rot,k}}{k_B} &= \frac{C_{v,k}^{\text{rot}}}{R} \\
\frac{c_{int,k}}{k_B} &= \frac{C_{v,k}}{R} - \frac{C_{v,k}^{\text{trans}}}{R} = \frac{C_{p,k}}{R} - \frac{5}{2}
\end{aligned} \tag{50}
$$

where $C_{v,k}^{\text{rot}}$ is obtained from (45) and $C_{v,k}^{\text{trans}} = \frac{3}{2}R$. The rotational relaxation collision number ξ_k for species k is given by (47). For monatomic species, $c_{rot,k}$ and $c_{int,k}$ are equal to zero such that the submatrix $L_{ij}^{01,01}$ can be written as a $(N - n^\star) \times (N - n^\star)$ matrix, with $n^\star$ the number of monatomic species.

C. Multicomponent thermodiffusion block matrix inverse

Two different formula for block matrix inverse can be used:

$$
\begin{aligned}
\begin{pmatrix} \mathbb{A} & \mathbb{B} \\ \mathbb{C} & \mathbb{D} \end{pmatrix}^{-1} &= \begin{pmatrix} \mathbb{A}^{-1} + \mathbb{A}^{-1}\mathbb{B}\boldsymbol{\mathcal{D}}^{-1}\mathbb{C}\mathbb{A}^{-1} & -\mathbb{A}^{-1}\mathbb{B}\boldsymbol{\mathcal{D}}^{-1} \\ -\boldsymbol{\mathcal{D}}^{-1}\mathbb{C}\mathbb{A}^{-1} & \boldsymbol{\mathcal{D}}^{-1} \end{pmatrix} \\
&\text{with} \qquad \boldsymbol{\mathcal{D}}^{-1} = (\mathbb{D} - \mathbb{C}\mathbb{A}^{-1}\mathbb{B})^{-1}
\end{aligned} \tag{51}
$$

or

$$
\begin{aligned}
\begin{pmatrix} \mathbb{a} & \mathbb{b} \\ \mathbb{c} & \mathbb{d} \end{pmatrix}^{-1} &= \begin{pmatrix} \boldsymbol{\mathcal{A}}^{-1} & -\boldsymbol{\mathcal{A}}^{-1}\mathbb{b}\mathbb{d}^{-1} \\ -\mathbb{d}^{-1}\mathbb{c}\boldsymbol{\mathcal{A}}^{-1} & \mathbb{d}^{-1} + \mathbb{d}^{-1}\mathbb{c}\boldsymbol{\mathcal{A}}^{-1}\mathbb{b}\mathbb{d}^{-1} \end{pmatrix} \\
&\text{with} \qquad \boldsymbol{\mathcal{A}}^{-1} = (\mathbb{a} - \mathbb{b}\mathbb{d}^{-1}\mathbb{c})^{-1}
\end{aligned} \tag{52}
$$

We can apply (51) to $\mathbb{L}$ defined as a block matrix:

$$
\begin{aligned}
\mathbb{A} &= \mathbb{L}^{00,00} & \mathbb{B} &= \begin{pmatrix} \mathbb{L}^{00,10} & \mathbb{0} \end{pmatrix} \\
\mathbb{C} &= \begin{pmatrix} \mathbb{L}^{10,00} \\ \mathbb{0} \end{pmatrix} & \mathbb{D} &= \begin{pmatrix} \mathbb{L}^{10,10} & \mathbb{L}^{10,01} \\ \mathbb{L}^{01,10} & \mathbb{L}^{01,01} \end{pmatrix}
\end{aligned} \tag{53}
$$

such that:

$$
\mathbb{L}^{-1} = \begin{pmatrix} \boldsymbol{\mathcal{L}}^{-1} + \boldsymbol{\mathcal{L}}^{-1}\mathbb{B}\boldsymbol{\mathcal{D}}^{-1}\mathbb{C}\boldsymbol{\mathcal{L}}^{-1} & -\boldsymbol{\mathcal{L}}^{-1}\mathbb{B}\boldsymbol{\mathcal{D}}^{-1} \\ -\boldsymbol{\mathcal{D}}^{-1}\mathbb{C}\boldsymbol{\mathcal{L}}^{-1} & \boldsymbol{\mathcal{D}}^{-1} \end{pmatrix} \tag{54}
$$

with $\boldsymbol{\mathcal{L}}^{-1}$ the inverse of $\mathbb{L}^{00,00}$, and where we need to invert the matrix $\boldsymbol{\mathcal{D}} = (\mathbb{D} - \mathbb{C}\boldsymbol{\mathcal{L}}^{-1}\mathbb{B})$ which can be written as a block matrix:

$$
\begin{aligned}
\mathbb{a} &= \mathbb{L}^{10,10} - \mathbb{L}^{10,00}\boldsymbol{\mathcal{L}}^{-1}\mathbb{L}^{00,10} & \mathbb{b} &= \mathbb{L}^{10,01} \\
\mathbb{c} &= \mathbb{L}^{01,10} & \mathbb{d} &= \mathbb{L}^{01,01}
\end{aligned} \tag{55}
$$

such that applying (52), we obtain:

$$
\boldsymbol{\mathcal{D}}^{-1} = \begin{pmatrix} (\boldsymbol{\mathcal{L}}_T)^{-1} & -(\boldsymbol{\mathcal{L}}_T)^{-1}\mathbb{L}^{10,01}(\mathbb{L}^{01,01})^{-1} \\ -\widetilde{\mathbb{L}}^{01,10}(\boldsymbol{\mathcal{L}}_T)^{-1} & \left[\mathbb{1} + \widetilde{\mathbb{L}}^{01,10}(\boldsymbol{\mathcal{L}}_T)^{-1}\mathbb{L}^{10,01}\right](\mathbb{L}^{01,01})^{-1} \end{pmatrix} \tag{56}
$$

where the inverse of the diagonal matrix $(\mathbb{L}^{01,01})^{-1}$ is straightforward, and where:

$$
\boldsymbol{\mathcal{L}}_T = \mathbb{L}^{10,10} - \mathbb{L}^{10,00}\boldsymbol{\mathcal{L}}^{-1}\mathbb{L}^{00,10} - \mathbb{L}^{10,01}\widetilde{\mathbb{L}}^{01,10} \tag{57}
$$

$$
\widetilde{\mathbb{L}}^{01,10} = (\mathbb{L}^{01,01})^{-1}\mathbb{L}^{01,10} \tag{58}
$$

In this way, the system $\mathbb{L}.\mathbf{a} = \mathbf{X}$ can be solved as $\mathbf{a} = \mathbb{L}^{-1}.\mathbf{X}$, where the inverse of the $(3N - n^\star) \times (3N - n^\star)$ matrix $\mathbb{L}$ only requires the inversion of two $N \times N$ matrices $\boldsymbol{\mathcal{L}}$ and $\boldsymbol{\mathcal{L}}_T$, since the inverse of the $(N - n^\star) \times (N - n^\star)$ diagonal matrix $\mathbb{L}^{01,01}$ is straightforward.

This is the general idea followed by Córdoba and Arias-Zugasti [16]. Moreover, they rewrite the problem $\mathbb{L}.\mathbf{a} = \mathbf{X}$ as $\mathbb{F}.\widetilde{\mathbf{a}} = \widetilde{\mathbf{X}}$:

$$
\begin{pmatrix} \mathbb{1} + \mathbb{A} & \mathbb{F}^{00,10} & \mathbb{0} \\ \mathbb{F}^{10,00} & \mathbb{F}^{10,10} & \mathbb{F}^{10,01} \\ \mathbb{0} & \mathbb{F}^{01,10} & \mathbb{1} \end{pmatrix} \begin{pmatrix} \widetilde{\mathbf{a}}_{00} \\ \widetilde{\mathbf{a}}_{10} \\ \widetilde{\mathbf{a}}_{01} \end{pmatrix} = \begin{pmatrix} \mathbf{0} \\ \widetilde{\mathbf{X}}_{10} \\ \widetilde{\mathbf{X}}_{01} \end{pmatrix} \tag{59}
$$

such that the inverse of the $(N - 1) \times (N - 1)$ matrix $\mathbb{1} + \mathbb{A}$ can be obtained following Arias-Zugasti *et al.* [14] or Naud and Arias-Zugasti [15]. The second matrix to be inverted is

$$
\mathbb{1} + \mathbb{A}_T = \mathbb{F}^{10,10} - \mathbb{F}^{10,00}(\mathbb{1} + \mathbb{A})^{-1}\mathbb{F}^{00,10} - \mathbb{F}^{10,01}\mathbb{F}^{01,10} \tag{60}
$$

where the system is properly rescaled such that the matrix inverse is approximated from Neumann series:

$$
\begin{aligned}
(\mathbb{1} + \mathbb{A}_T)_{ij}^{-1} =& \left(\sum_{r=0}^{\infty} (-\mathbb{A}_T)^r \right)_{ij} \\
=& \delta_{ij} - A_{T,ij} + \sum_k A_{T,ik}A_{T,kj} - ...
\end{aligned} \tag{61}
$$

The solution of system (59):

$$\widetilde{\mathbf{a}}_{10} = -\left(\mathbb{1} + \mathbb{A}_T\right)^{-1}\left(\mathbb{F}^{10,01}\widetilde{\mathbf{X}}_{01} - \widetilde{\mathbf{X}}_{10}\right) \tag{62}$$

$$\widetilde{\mathbf{a}}_{01} = \widetilde{\mathbf{X}}_{01} - \mathbb{F}^{01,10}\widetilde{\mathbf{a}}_{10} \tag{63}$$

$$\widetilde{\mathbf{a}}_{00} = -\left(\mathbb{1} + \mathbb{A}\right)^{-1}\mathbb{F}^{00,10}\widetilde{\mathbf{a}}_{01} \tag{64}$$

can then be approximated using the Neumann series (61) truncated at order n:

$$\widetilde{\mathbf{a}}_{10} \approx \sum_{r=0}^{n} \mathbf{w}^{(r)} \tag{65}$$

where:

$$w_i^{(0)} = \widetilde{X}_{10,i} - \sum_k F_{ik}^{10,01}\widetilde{X}_{01,k} \tag{66}$$

$$w_i^{(r)} = w_i^{(r-1)} + \sum_j \left(-F_{ij}^{10,10} + \mathcal{G}_{ij} + \mathcal{H}_{ij}\right) w_j^{(r-1)} \tag{67}$$

$$\text{with} \quad \mathcal{G}_{ij} = \sum_k \left(F_{ik}^{10,00} \sum_\ell \left(\mathbb{1} + \mathbb{A}\right)^{-1}_{k\ell} F_{\ell j}^{00,10} \right)$$

$$\text{and} \quad \mathcal{H}_{ij} = \sum_k F_{ik}^{10,01} F_{kj}^{01,10}$$

D. Mixture-averaged approximation

As in A, we detail here the transport properties for the mixture-averaged approximation as implemented in [5]. When the mixture-averaged approximation is used, the diffusion fluxes (1) are written as:

$$\rho \mathbf{V}_i Y_i = -\rho \frac{W_i}{\overline{W}} D_i^{(\mathrm{MA})} \nabla X_j - \rho Y_i D_{T,i}^{(\mathrm{MA})} \nabla \ln T \tag{68}$$

and a correction velocity $\mathbf{V}_c$ is added to species diffusive velocity $\mathbf{V}_i$ in order to ensure that the net species diffusion flux is zero:

$$\mathbf{V}_c = \sum_j^N Y_j \mathbf{V}_j \tag{69}$$

In this case, the effective diffusion coefficient $D_i^{(\mathrm{MA})}$ of the i-th species into the mixture is approximated as:

$$D_i^{(\mathrm{MA})} = \frac{1 - Y_i}{\sum_{j \neq i} X_j \Big/ \mathcal{D}_{ji}} \tag{70}$$

The thermal diffusion coefficients $D_{T,i}^{(\mathrm{MA})}$ are considered to be non-zero for "light" species only (typically H, He and H_2). They are obtained as:

$$D_{T,i}^{(\mathrm{MA})} = D_i^{(\mathrm{MA})} \sum_k \theta_{ik} X_k \tag{71}$$

with

$$\theta_{ik} = \frac{15}{2} \frac{\left(2A_{ik}^* + 5\right)\left(6C_{ik}^* - 5\right)}{A_{ik}^*\left(16A_{ik}^* - 12B_{ik}^* + 55\right)} \frac{W_i - W_k}{W_i + W_k} \tag{72}$$

The thermal conductivity of the mixture is evaluated as:

$$\lambda^{(\mathrm{MA})} = \frac{1}{2}\left[\sum_k X_k \lambda_k + \frac{1}{\sum_k X_k/\lambda_k}\right] \tag{73}$$

where the pure thermal conductivities λ_k are assumed to be composed of transitional, rotational and vibrational contributions and are obtained from the pure viscosities η_k as [32]:

$$\lambda_k = \frac{\eta_k}{W_k}\left(f_k^{\mathrm{trans}} C_{v,k}^{\mathrm{trans}} + f_k^{\mathrm{rot}} C_{v,k}^{\mathrm{rot}} + f_k^{\mathrm{vib}} C_{v,k}^{\mathrm{vib}}\right) \tag{74}$$

Following Warnatz [32]:

$$\begin{aligned} f_k^{\mathrm{trans}} &= \frac{5}{2}\left(1 - \frac{2}{\pi}\frac{C_{v,k}^{\mathrm{rot}}}{C_{v,k}^{\mathrm{trans}}}\frac{A_k}{B_k}\right) \\ f_k^{\mathrm{rot}} &= \frac{\rho \mathcal{D}_{kk}}{\eta_k}\left(1 + \frac{2}{\pi}\frac{A_k}{B_k}\right) \quad \text{and} \quad f_k^{\mathrm{vib}} = \frac{\rho \mathcal{D}_{kk}}{\eta_k} \end{aligned} \tag{75}$$

with

$$A_k = \frac{5}{2} - \frac{\rho \mathcal{D}_{kk}}{\eta_k} \quad \text{and} \quad B_k = \xi_k + \frac{2}{\pi}\left(\frac{5}{3}\frac{C_{v,k}^{\mathrm{rot}}}{R} + \frac{\rho \mathcal{D}_{kk}}{\eta_k}\right) \tag{76}$$

where η_k, $\mathcal{D}_{kk}$ and ξ_k are obtained from (36), (37) and (47), respectively, and where $C_{v,k}^{\mathrm{trans}}$, $C_{v,k}^{\mathrm{rot}}$ and $C_{v,k}^{\mathrm{vib}}$ are defined in (44) and (45).

As for species viscosities and binary diffusion coefficients, Equations (72) and (74) are computed over a given range of temperatures $[T_{\min}, T_{\max}]$, and a polynomial fit algorithm is used in order to obtain an approximation of the properties [5]:

$$\begin{aligned} \theta_{ik} &= \sum_{n=1}^{4} \alpha_{n,ik} T^{n-1} \\ \ln \lambda_k &= \sum_{n=1}^{4} \beta_{n,k} (\ln T)^{n-1} \end{aligned} \tag{77}$$

such that (72) and (74) are only calculated once over the temperature range $[T_{\min}, T_{\max}]$ at the begin of the calculation in order to evaluate the coefficients $\alpha_{n,ik}$ and $\beta_{n,k}$.

E. Skeletal mechanism for methane oxidation

In Table 6, we give the 77 reactions of the 26-species skeletal mechanism considered, where reactions 31, 41, 64, 67, 69, 76 and 77 are simply considered as forward reactions. The reaction rates are obtained from [28] (where reactions 14, 16 and 19 are duplicate reactions).

References

[1] L. Monchick, E.A. Mason, Transport Properties of Polar Gases, *J. Chem. Phys.* **35** (1961) 1676–1697.

[2] E.A. Mason, L. Monchick, Heat conductivity of polyatomic and polar gases, *J. Chem. Phys.* **36** (1962) 1622–1639.

[3] L. Monchick, K.S. Yun, E.A. Mason, Formal kinetic theory of transport phenomena in polyatomic gas mixtures, *J. Chem. Phys.* **39** (1963) 654–669.

Table 6: 26-species skeletal mechanism for methane oxidation.

1. $H+O_2 \rightleftharpoons OH+O$	40. $CH_3+O \rightleftharpoons CH_2O+H$
2. $H_2+O \rightleftharpoons OH+H$	41. $CH_3+T\text{-}CH_2 \rightarrow C_2H_4+H$
3. $H_2+OH \rightleftharpoons H_2O+H$	42. $CH_3+HO_2 \rightleftharpoons CH_3O+OH$
4. $H_2O+O \rightleftharpoons 2OH$	43. $CH_3+O_2 \rightleftharpoons CH_2O+OH$
5. $2H+M \rightleftharpoons H_2+M$	44. $CH_3+O_2 \rightleftharpoons CH_3O+O$
6. $H+OH+M \rightleftharpoons H_2O+M$	45. $2CH_3 \rightleftharpoons C_2H_5+H$
7. $2O+M \rightleftharpoons O_2+M$	46. $H+CH_3(+M) \rightleftharpoons CH_4(+M)$
8. $H+O+M \rightleftharpoons OH+M$	47. $2CH_3(+M) \rightleftharpoons C_2H_6(+M)$
9. $H+O_2(+M) \rightleftharpoons HO_2(+M)$	48. $S\text{-}CH_2+O_2 \rightleftharpoons CO+OH+H$
10. $HO_2+H \rightleftharpoons 2OH$	49. $S\text{-}CH_2+M \rightleftharpoons T\text{-}CH_2+M$
11. $HO_2+H \rightleftharpoons H_2+O_2$	50. $T\text{-}CH_2+O \rightleftharpoons CO+2H$
12. $HO_2+H \rightleftharpoons H_2O+O$	51. $T\text{-}CH_2+O \rightleftharpoons CO+H_2$
13. $HO_2+O \rightleftharpoons OH+O_2$	52. $T\text{-}CH_2+O_2 \rightleftharpoons CO_2+H_2$
14. $HO_2+OH \rightleftharpoons H_2O+O_2$	53. $T\text{-}CH_2+O_2 \rightleftharpoons CO+OH+H$
15. $2OH(+M) \rightleftharpoons H_2O_2(+M)$	54. $CH_3O+O_2 \rightleftharpoons CH_2O+HO_2$
16. $2HO_2 \rightleftharpoons H_2O_2+O_2$	55. $CH_3O+M \rightleftharpoons CH_2O+H+M$
17. $H_2O_2+H \rightleftharpoons HO_2+H_2$	56. $C_2H_6+H \rightleftharpoons C_2H_5+H_2$
18. $H_2O_2+H \rightleftharpoons H_2O+OH$	57. $C_2H_6+O \rightleftharpoons C_2H_5+OH$
19. $H_2O_2+OH \rightleftharpoons H_2O+HO_2$	58. $C_2H_6+OH \rightleftharpoons C_2H_5+H_2O$
20. $H_2O_2+O \rightleftharpoons HO_2+OH$	59. $C_2H_6(+M) \rightleftharpoons C_2H_5+H(+M)$
21. $CO+OH \rightleftharpoons CO_2+H$	60. $C_2H_5+H \rightleftharpoons C_2H_4+H_2$
22. $HCO+M \rightleftharpoons CO+H+M$	61. $C_2H_5(+M) \rightleftharpoons C_2H_4+H(+M)$
23. $HCO+H \rightleftharpoons CO+H_2$	62. $C_2H_4+H \rightleftharpoons C_2H_3+H_2$
24. $HCO+OH \rightleftharpoons CO+H_2O$	63. $C_2H_4+OH \rightleftharpoons C_2H_3+H_2O$
25. $HCO+O_2 \rightleftharpoons CO+HO_2$	64. $C_2H_4+O \rightarrow CH_3+HCO$
26. $HCO+CH_3 \rightleftharpoons CO+CH_4$	65. $C_2H_3+H \rightleftharpoons C_2H_2+H_2$
27. $CH_2O+H \rightleftharpoons HCO+H_2$	66. $C_2H_3(+M) \rightleftharpoons C_2H_2+H(+M)$
28. $CH_2O+O \rightleftharpoons HCO+OH$	67. $C_2H_3+O_2 \rightarrow CH_2CO+H+O$
29. $CH_2O+OH \rightleftharpoons HCO+H_2O$	68. $C_2H_3+O_2 \rightleftharpoons C_2H_2+HO_2$
30. $CH_2O+O_2 \rightleftharpoons HCO+HO_2$	69. $C_2H_2+OH \rightarrow CH_2CO+H$
31. $CH_2O+HO_2 \rightarrow HCO+H_2O_2$	70. $CH_2CO+H \rightleftharpoons CH_3+CO$
32. $CH_4+H \rightleftharpoons H_2+CH_3$	71. $CH_3OH(+M) \rightleftharpoons CH_3+OH(+M)$
33. $CH_4+OH \rightleftharpoons H_2O+CH_3$	72. $CH_2OH+H \rightleftharpoons CH_2O+H_2$
34. $CH_4+O \rightleftharpoons CH_3+OH$	73. $CH_2OH+H \rightleftharpoons CH_3+OH$
35. $CH_4+O_2 \rightleftharpoons CH_3+HO_2$	74. $CH_2OH+O_2 \rightleftharpoons CH_2O+HO_2$
36. $CH_4+HO_2 \rightleftharpoons CH_3+H_2O_2$	75. $CH_2OH+M \rightleftharpoons CH_2O+H+M$
37. $CH_3+H \rightleftharpoons T\text{-}CH_2+H_2$	76. $CH_3O+M \rightarrow CH_2OH+M$
38. $CH_3+H \rightleftharpoons S\text{-}CH_2+H_2$	77. $CH_3OH+OH \rightarrow CH_2OH+H_2O$
39. $CH_3+OH \rightleftharpoons S\text{-}CH_2+H_2O$	

[4] G. Dixon-Lewis, Flame structure and flame reaction kinetics II. Transport phenomena in multicomponent systems, *Proc. R. Soc. A.* **304** (1968) 111–135.

[5] R.J. Kee, G. Dixon-Lewis, J. Warnatz, M.E. Coltrin, J.A. Miller, H.K. Moffat, *A fortran computer code package for the evaluation of gas-phase, multi-component transport properties*, Sandia National Laboratories Report, SAND86-8246B, 1998.

[6] V. Giovangigli, Convergent iterative Methods for Multicomponent Diffusion, *Impact Comput. Sci. Eng.* **3** (1991) 244–276.

[7] A. Ern, V. Giovangigli, Fast and accurate multicomponent transport property evaluation, *J. Comput. Phys.* **406** (1995) 105–116.

[8] A. Ern, V. Giovangigli, Multicomponent transport algorithms, *Lecture Notes in Physcis Monographs*, Springer, Berlin, Heidelberg, 2008.

[9] Y. Xin, W. Liang, W. Liu, T. Lu, C.K. Law, A reduced multicomponent diffusion model, *Combust. Flame* **162** (2015) 68–74.

[10] S. Ambikasaran, K. Narayanaswamy, An accurate, fast, mathematically robust, universal, non-iterative algorithm for computing multi-component diffusion velocities, *Proc. Comb. Inst.* **36** (2017) 507–515.

[11] W. Sun, Y. Ju, A multi-timescale and correlated dynamic adaptive chemistry and transport (CO-DACT) method for computationally efficient modeling of jet fuel combustion with detailed chemistry and transport, *Combust. Flame* **184** (2017) 297–311.

[12] A.J. Fillo, J. Schlup, G. Beardsell, G. Blanquart, K.E. Niemeyer, A fast, low-memory, and stable algorithm for implementing multicomponent transport in direct numerical simulations, J. Comput. Phys. **406** (2020) 109185.

[13] A.J. Fillo, J. Schlup, G. Blanquart, K.E. Niemeyer, Assessing the impact of multicomponent diffusion in direct numerical simulations of premixed, high-Karlovitz, turbulent flames, *Combust. Flame* **223** (2021) 216–229.

[14] M. Arias-Zugasti, P.L. Garcia-Ybarra, J.L. Castillo, Efficient calculation of multicomponent diffusion fluxes based on kinetic theory, *Combust. Flame*, **163** (2016) 540–556.

[15] B. Naud, M. Arias-Zugasti, Accurate multicomponent Fick diffusion at a lower cost than mixture-averaged approximation: validation in steady and unsteady counterflow flamelets, *Combust. Flame*, **219** (2020) 120–128.

[16] O. Córdoba, M. Arias-Zugasti Accurate and efficient calculation of multicomponent thermal diffusion coefficients and partial thermal conductivity based on kinetic theory, *Combust. Flame* **244** (2022) 112202.

[17] R.J. Kee, J.A. Miller, G.H. Evans, G. Dixon-Lewis, A computational model of the structure and extinction of strained, opposed flow, premixed methane-air flames, *Proc. Comb. Inst.* **22** (1989) 1479–1494.

[18] A.E. Lutz, R.J. Kee, J.F. Grcar, F.M. Rupley, *OPPDIF: A Fortran program for computing opposed-flow diffusion flames*, Sandia National Laboratories Report, SAND96-8243, 1997.

[19] B. Naud, R., Novella, J.-M. Pastor, J.F. Winklinger, RANS modelling of a lifted H_2/N_2 flame using an unsteady flamelet progress variable approach with presumed PDF, *Combust. Flame* **162** (2015) 893–906.

[20] S. Gordon, B.J. McBride, *Computer Program for Calculation of Complex Chemical Equilibrium Compositions, Rocket Performance, Incident and Reflected Shocks, and Chapman-Jouquet Detonations*, NASA-SP-273, 1971.

[21] J.F. Grcar, *The Twopnt Program for Boundary Value Problems*, Sandia National Laboratories Report, SAND91-8230, 1992.

[22] L.R. Petzold, *A Description of DASSL: A Differential/Algebraic System Solver*, Sandia National Laboratories Report, SAND82-8637, 1982.

[23] J.O. Hirschfelder, C.F. Curtiss, R.B. Bird, *The molecular theory of gases and liquids*, Wiley, 1954.

[24] R. Cabra, J.-Y. Chen, R.W. Dibble, A.N. Karpetis, R.S. Barlow, Lifted methane–air jet flames in a vitiated coflow, *Combust. Flame* **143** (2005) 491–506.

[25] B.B. Dally, A.R. Masri, R.S. Barlow, G.J. Fiechtner. Instantaneous and mean compositional structure of bluff-body stabilized nonpremixed flames, *Combust. Flame* **114** (1998) 119–148.

[26] M. Zhou, F. Yan, L. Ma, P. Jiang, Y. Wang, S.H. Chung, Chemical speciation and soot measurements in laminar counterflow diffusion flames of ethylene and ammonia mixtures, *Fuel* **308** (2022) 122003.

[27] A. Stagni, D. Brignoli, M. Cinquanta, A. Cuoci, A. Frassoldati, E. Ranzi, T. Faravelli The influence of low-temperature chemistry on partially-premixed counterflow n-heptane/air flames, *Combust. Flame* **188** (2018) 440–452.

[28] Chemical-Kinetic Mechanisms for Combustion Applications, San Diego Mechanism web page, Mechanical and Aerospace Engineering (Combustion Research), University of California at San Diego (http://combustion.ucsd.edu).

[29] B. Naud Skeletal mechanism and augmented reduced mechanisms for methane oxidation, *Proceedings of the Mediterranean Combustion Symposium 11*. (2019).

[30] Y. Wang, A. Raj, S.H. Chung, A PAH growth mechanism and synergistic effect on PAH formation in counterflow diffusion flames, *Combust. Flame* **160** (2013) 1667–1676.

[31] M. Pelucchi, M. Bissoli, C. Cavallotti, A. Cuoci, T. Faravelli, A. Frassoldati, E. Ranzi, A. Stagni, Improved kinetic model of the low-temperature oxidation of n-heptane, *Energy Fuels* **28** (2014) 7178—7193.

[32] J. Warnatz, *Influence of Transport Models and Boundary Conditions on Flame Structure*, Friedr., Vieweg, Wiesbaden, 1982.

[33] T.R. Marrero, E.A. Mason, Gaseous Diffusion Coefficients *J. Phys. Chem. Ref. Data* 1, 3 (1972); https://doi.org/10.1063/1.3253094

[34] J.G. Parker, Rotational and Vibrational Relaxation in Diatomic Gases, *Phys. Fluids* **2** (1959) 449–462.

[35] C.C. Brau, R.M. Jonkman, Classical Theory of Rotational Relaxation in Diatomic Gases, *J. Chem. Phys.* **52** (1970) 477–484.